CURRENTS GENERATED BY UPSIDE-DOWN JELLYFISH: IMPLICATIONS FOR SUSPENSION FEEDING AND PORE WATER PUMPING

By

MANIKANTAM GOUD GADDAM

Bachelor of Engineering in Mechanical Engineering

Osmania University

Hyderabad, India

2014

Submitted to the Faculty of the
Graduate College of the
Oklahoma State University
in partial fulfillment of
the requirements for
the Degree of
MASTER OF SCIENCE
December, 2016

CURRENTS GENERATED BY UPSIDE-DOWN JELLYFISH: IMPLICATIONS FOR SUSPENSION FEEDING AND PORE WATER PUMPING

Thesis Approved:

Dr. Arvind Santhanakrishnan

Thesis Adviser

Dr. Brian Elbing

Dr. Khaled Sallam

ACKNOWLEDGEMENTS

I sincerely thank my graduate advisor Dr. Arvind Santhanakrishnan for his encouragement and support throughout the research project. I thank my committee members Dr. Brian Elbing and Dr. Khaled Sallam for their valuable suggestions and for reviewing my thesis.

I extend my thanks to Matthew-Takyi-Micah, Naman Mathur, Jullian Fields, Milad Samaee, Hong Kuan Lai and Vishwa Teja Kasoju for their support in setting up the equipment in the Laboratory and *Cassiopea* spp. maintenance. I also thank Dr. Charlotte Fore and Beth Powers for valuable guidance throughout my Masters.

Finally, I thank my parents Mr. & Mrs. Papaiah Gaddam and my family members for their immense love and support throughout my journey.

Name: MANIKANTAM GOUD GADDAM

Date of Degree: DECEMBER, 2016

Title of Study: CURRENTS GENERATED BY UPSIDE-DOWN JELLYFISH: IMPLICATIONS FOR SUSPENSION FEEDING AND PORE WATER PUMPING

Major Field: MECHANICAL AND AEROSPACE ENGINEERING

Abstract: The bottom or benthic boundary layer (BBL) of the oceans presents challenging conditions for foraging, on account of ambient flows as slow as few centimeters per second. Several marine invertebrates (such as sponges) have adapted to life in the BBL by generating steady currents for use in feeding on suspended particulate prey. Low-speed flows also limit nutrient cycling via pore water uptake. We examine how unsteady jets can impact suspension feeding and pore water entrainment using a model organism: the upside-down *Cassiopea* jellyfish. *Cassiopea* individuals are found attached to the substrate in shallow ocean waters such as mangrove swamps, with their bells and oral arms pointing upwards to the free surface. Through periodic contractions and relaxations of their bell margin, these sessile organisms generate vortex-dominated jets for feeding and nutrient exchange. We examined pulsing kinematics, flows, and transport characteristics in *Cassiopea* using videography, 2D particle image velocimetry (PIV) and planar laser induced fluorescence (PLIF). Multiple individuals with bell diameters ranging from 2 cm to 7 cm were investigated in laboratory settings under varying background flows. Pulsing frequency was observed to generally decrease with increasing bell diameter. Near-field PIV measurements showed that the ambient water was drawn toward the bell margin during each contraction to form a starting vortex. Continuous upward jets were formed after flow entrained by the bell was directed through the oral arms. Under background flow with mean velocity of 2 cm s^{-1}, the penetration depth of the organism-induced jet decreased with increasing bell diameter. However, volumetric fluxes in the same background flow condition increased with increasing bell diameter. PLIF measurements showed suction pumping of fluorescent dye initially located 2 cm below the substrate. Coherent flow structures formed during bell contraction were broken into small-scale structures when the jet was advected upward through the oral arms. Smaller individuals with higher pulsing frequency showed closer placement of vortices from multiple pulsing cycles that aided in augmenting concentration flux. In contrast, larger medusae with lower pulsing frequency appear to potentially benefit from increased time-scale for suspension feeding and mixing of pore water, on account of their wider and slower jets.

TABLE OF CONTENTS

Chapter Page

LST OF FIGURES

CHAPTER I

INTRODUCTION

1.1 Motivation

All benthic living organisms (benthos) require energy to sustain functions such as respiration, uptake of nutrients, locomotion and excretion. Autotrophic organisms produce organic compounds (carbohydrates, fats and proteins) without needing a living source of energy or organic carbon. In contrast, heterotrophic organisms depend on autotrophic organisms for carbon fixation and can also feed other organisms using variety of techniques. Depending on type of predation, feeding mechanisms are classified into suction feeding, ram feeding, pivot feeding, protrusion feeding and suspension feeding [1]. In the benthic zone, where the water velocity can be as low as a few cm/s [2], sessile organisms typically use suspension feeding mechanism. Suspension feeding is broadly classified into active and passive categories based on whether energy is expended by the organism to drive fluid through its feeding appendages [3]. Active suspension feeding typically relies on using organism-induced currents for sampling the water. Previous research on benthic organisms such as bivalves [4, 5], sponges [6, 7], have investigated the use of steady, organism-induced currents for the functions of active suspension feeding, exchanging of nutrients, gases and excreta. Laboratory flume and wave tank experiments using these organisms showed an increase in the prey capture rate in oscillating flow conditions compared to unidirectional flow [8]. Further, in colonies of flexible suspension feeders, particle capture was found to depend mostly on parameters like fluid velocity, colony orientation and fluid re-sampling [8]. The flow velocity over colonies of suspension feeders was dampened

to increase the capture rates [9]. In contrast to these studies, little is known on the physical mechanisms underlying suspension feeding in organisms that use unsteady currents. We address this paucity in understanding by using a model organism, the upside-down jellyfish, *Cassiopea*, where unsteady bell pulsations drive currents for the functions of suspension feeding, excretion, and exchanging gas and nutrients.

1.2 Ecological Significance

Gelatinous zooplanktons (such as jellyfish, ctenophores) constitute a significant portion of the biomass in the pelagic zone of the oceans [10]. According to recent studies, there has been notable increase in the frequency and distribution of gelatinous zooplankton [11]. The population increase of gelatinous zooplankton can potentially affect their ecosystem via altering the community structure [12]. Although most of these zooplanktons have short life spans, they can increase their population at high growth rates [13]. Recent investigations in near shore waters of Florida and the northern Gulf of Aqaba, Red Sea showed the decline in the health of the coral reef system due to the increase in nutrient levels [14, 15]. There is thus a critical need for studying such bio-physical interactions in gelatinous zooplankton, for the purposes of identifying the factors that engender these population shifts.

Benthic jellyfish such as *Cassiopea* have been noted to appear in patchy aggregations in costal ecosystems. Localized blooms of *Cassiopea* medusa have been observed near urban areas where human disturbances such as marine construction and artificial enrichment of nutrients can occur. In contrast to studies of larger pelagic jellyfish blooms, it is unclear how aggregations of benthic jellyfish can alter ecosystem function and community structure. This study will aim to provide insight into how *Cassiopea* individuals can alter their local flow environment.

1.3 Specific Aims

The broad goal of this study is to examine the feeding and exchange currents generated by *Cassiopea* individuals. The first objective will characterize the currents generated by medusae of varying bell sizes under different background flows conditions. The second objective will examine the relation between *Cassiopea* bell diameter, pulsing frequency and pore water release into water column. These objectives will be achieved using the following specific aims (SAs).

SA 1: Quantify bell kinematics of *Cassiopea* individuals of varying sizes and examine how the currents generated by the organisms interact with continuous background flows. Multiple *Cassiopea* individuals of bell diameters ranging from 2-7 cm will be examined in a laboratory flow tank under continuous background flows ranging in magnitude from 0-2 cm/s. Videography recordings will be used for bell kinematics calculations and PIV will be used to visualize the flow structures formed by pulsing *Cassiopea* and quantitatively describe how organism-induced jets interact with background flows. SA1 will be discussed in Chapter III.

SA 2: Quantify pore water pumping characteristics by *Cassiopea* individuals of varying sizes under no background flow conditions. Sand beds will be prepared in a laboratory aquarium such that the bottom layer of sand is colored with fluorescent Rhodamine WT dye. PLIF measurements will be acquired on *Cassiopea* individuals introduced to this aquarium under no background flow conditions. The recorded images will be processed to obtain contour maps of normalized concentration. PIV measurements will also be conducted under identical conditions to obtain the relation between bell diameters, pulsing frequency and current velocities. SA2 will be discussed in Chapter IV.

The relationships between *Cassiopea* individual size (bell diameter), pulsing frequency, current velocity magnitudes, hydrodynamic forces and concentrations in the water column will be

obtained. The outcomes of this study will provide an overall understanding of how bell pulsations of *Cassiopea* can impact suspension feeding and pore water release.

CHAPTER II

LITERATURE REVIEW

2.1 Feeding Mechanisms

Food is the basic requirement for all living organisms (both aquatic and terrestrial) for all physiological processes. Living organisms which are autotrophic can prepare their own food while the heterotrophic depends on other living organisms for food. Heterotrophic organisms use different types of techniques for prey capture. When we consider the aquatic zone, different feeding mechanisms are classified based on type of predation. They are suction feeding, ram feeding, pivot feeding, protrusion feeding and suspension feeding [1]. In Suction feeding, predator organisms intake the water parcel containing the prey and ingest it. This prey intake occurs due to the pressure difference caused by mouth expansion. An example includes *Osteichthyes* using mechanical linkage for opening the buccal cavity. In ram feeding, predators open their mouths, move forward towards the prey, and engulf the fluid containing the prey. One example includes herring feeding on copepods. In pivot feeding, organisms open their mouths towards the prey by upward turning of the head. E.g., *Hippocampus* sp. feeding on copepods. In protrusion feeding, organisms extend their mouths towards the prey through mechanical linkages. E.g., *Epibulus insidiator*. Finally, in suspension feeding method, organisms select particulate food matter from flows. Water flow is generally created by the organism itself or by an external source and the prey particles are captured. Some examples are sponges, bivalves.

2.2 Classification of Suspension Feeding

Based on the source of energy required to drive the fluid through the suspension feeding structures, suspension feeding can be classified into active and passive suspension feeding. In active suspension feeding, the metabolic energy is used to drive the currents through feeding structures while in passive suspension feeding, they depend on the ambient flow to drive the water past the feeding structures [16] .

2.3 Particle Capture Mechanisms in Suspension Feeding Organisms

Prey is captured by suspension feeders in six different ways either alone or in combination. These include 1) scan and trap, 2) sieving, 3) direct interception, 4) inertial impaction, 5) gravitational deposition and 6) diffusive deposition [16]. In *scan and trap*, when the prey reaches a detectable distance, predators alter the fluid motion causing the prey to isolate from parcels of fluid and reach its feeding structures. E.g., *Flustrellidra hispida*. In *sieving* mechanism prey particles are made to pass through mesh-like structures created by organisms with their feeding elements. Particles less than the mesh size escape while the prey with larger diameters than the mesh are captured. These captured prey are ensured to be retained by producing a sticky mucus at the feeding structures. E.g., *Cassiopea* medusa. In *direct interception*, particles follow the streamline path and when they reach one radial distance from the feeding structure then prey is captured by touching and sticking to the feeding element. Here the particle is neutrally buoyant and follows the free streamline. E.g., *Ophipholus aculeate*. In *Inertial impaction,* prey particle density is different from the fluid density and as the fluid changes its direction to cross the feeding structures, the particles move towards the feeding structures because of the inertial force. If the particle reaches one radial distance, then it is captured by the feeding element. An example includes *Ophipholus aculeate*. *Gravitational deposition* is same as inertial impaction in which the prey particles are deposited on the feeding structure mainly due to gravitational force acting on

them. In *diffusive deposition,* the prey particle follows a random path in the ambient flow and gets captured to a feeding structure.

2.4 Previous Work on Suspension Feeding Benthic Invertebrates

2.4.1 Sponges

Sponges have choanocytes with flagellum which help in pumping the water through microvilli (acting as a sieve) that capture the bacteria or prey. Feeding happens when the ambient flow containing bacteria enters into the sponge body through small openings, called ostia, present on the surface as shown in Figure 1. This water flows through the inhalant canal system to the water pumping units, choanocyte chambers, where the prey is captured [17, 18]. Then the filtered water leaves the choanocyte through exhalant canal system and finally through the osculum on the surface. All the pumping units (choanocytes) operate parallel and with same flow rate and pressure rise [19, 20] illustrating that sponges use steady currents for prey capturing.

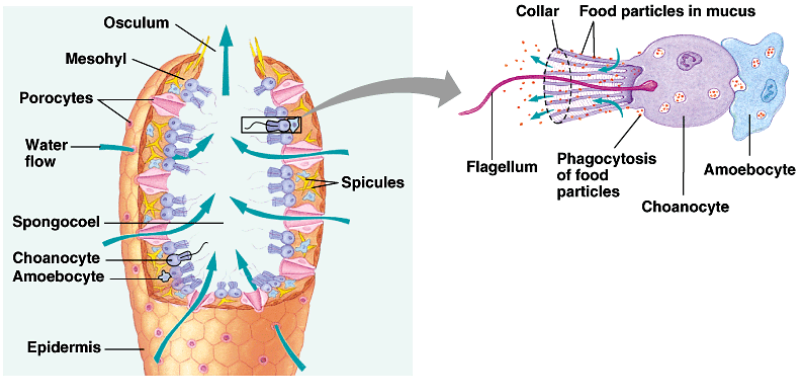

Figure 1.Suspension feeding mechanism in sponges [21].

2.4.2 Bivalves

Particles are separated at the entrance of the canal from main stream and transported onto the frontal surface of the laterofrontal cirri. These food particles are stopped at the inter-filament gap and are then transported to the grill filament. These food particles are then transported towards the marginal food groove by frontal cilia as shown in Fig 2. Experimental investigation showed production of steady currents by bivalves for food intake [22, 23].

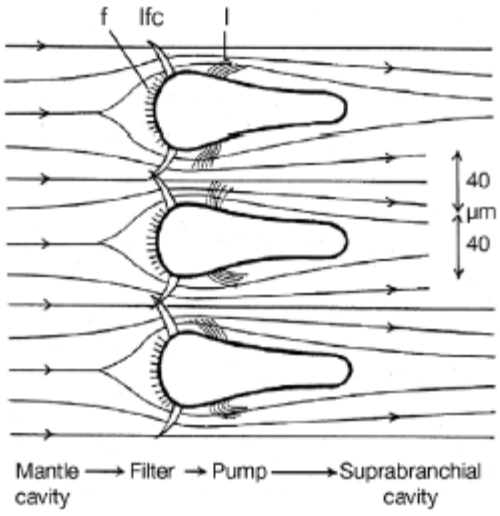

Figure 2. Cross section of three grill filaments in the bivalve *Mytilus edulis* [19].

2.4.3 Summary

These experimental works showed the production of steady currents for prey capture by benthic living organisms. But there are few other living organisms which produce unsteady currents for feeding and exchange gases; the information on such model living organisms was limited. Next a model organism, known as the upside-down jellyfish, *Cassiopea* spp., that uses unsteady currents for feeding and exchange gases, will be presented.

2.5 *Cassiopea* spp.

The genus *Cassiopea* belong to the Kingdom Animalia, with the Phylum Cnidaria, the Class Scyphozoa, the Order Rhizostomeae and the Family Cassiopeidae. There are eight species in the *Cassiopea* genus. They are *Cassiopea andromeda*, *Cassiopea depressa*, *Cassiopea frondosa*, *Cassiopea medusa*, *Cassiopea mertensi*, *Cassiopea ndrosia*, *Cassiopea oranta* and *Cassiopea xamachana*.

2.5.1 Morphology

Cassiopea medusa, called the upside down jellyfish, stays in patchy aggregations with density ranging up to 31 individuals m^{-2}[24]. They are found in benthic habitats such as mangrove swamps, coral reefs and seagrass meadows with low ambient flows [25]**.** The morphology of the *Cassiopea* spp. includes an umbrella-shaped bell and eight oral arms with appendages (secondary mouths) fused over the central mouth [26] as shown in Fig 3. These organisms have sessile and non-swimming style and always attached with their bell against the substrate and oral arms pointing towards the sunlight [27]. These are functionally autotrophic animals (i.e. can prepare their own food by photosynthesis and also depend on living organisms) and depend on the symbiotic algae Symbiodinium, also known as "zooxanthellae", present in their oral arms for meeting their carbon requirement. Autotrophic nutrition is also achieved by feeding on small living organisms such as copepods [28].The carbon required by *Cassiopea* individuals is mostly attained through zooxanthella and nutrients through feeding and diffusion processes [29].

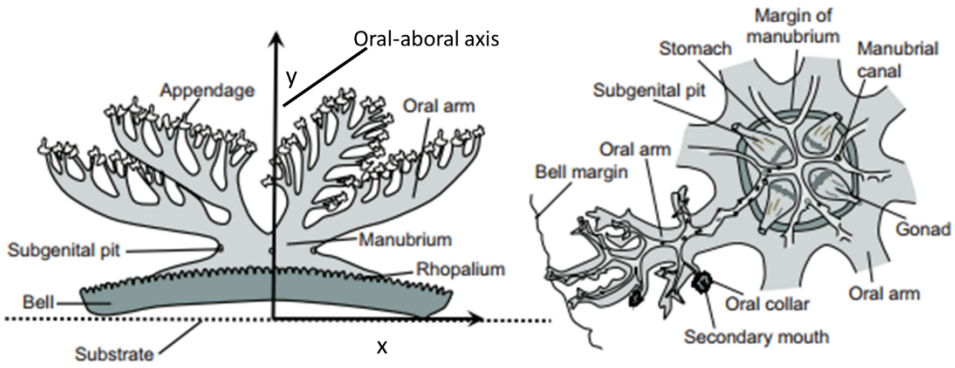

Figure 3. Morphology of *Cassiopea* in left side and top view on the right side [modified from Santhanakrishnan et al., 2012].

2.5.2 Life cycle of *Cassiopea*

The *Cassiopea* spp. are dioecious (having male and female organs in different individuals) and their biological life cycle starts with alternation between the medusa stage and the polyp stage [30] as shown in Fig 4. Sperm released by the individual fertilize the eggs of the nearby female. These fertilized eggs are safely transported to knob-shaped tentacles present at the center of the female. These eggs are then developed into larvae and hatch out to give planulae after metamorphosis. These planulae settle on hard surface and metamorphose to a polyp with tentacles called scyphistomae which can reproduce asexually through budding. These buds settle and form scyphistomae. When the habitat temperature reaches 20^{o} C and higher, this scyphistomaestrobilate (type of asexual reproduction consisting of spontaneous transverse repetition of body plans) happens to transform buds in to the medusa after acquiring certain species of zooxanthellae [31].

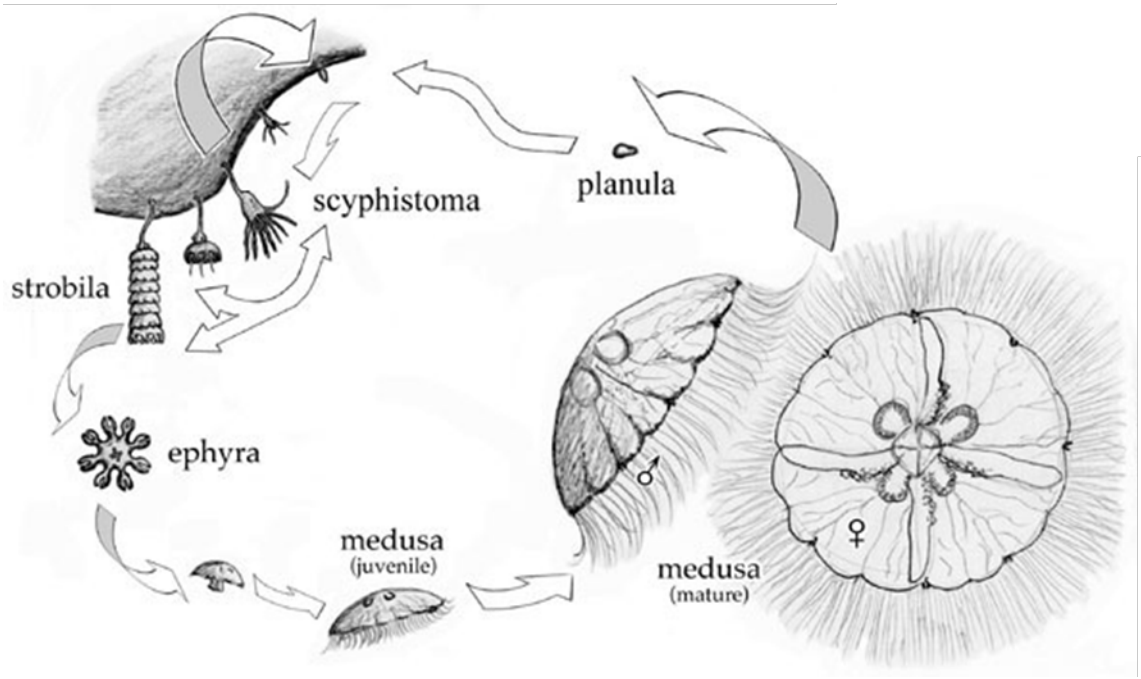

Figure 4. Life Cycle of *Cassiopea* medusa [32].

2.6 Previous Research on *Cassiopea* spp.

Several recent studies examined the currents generated by *Cassiopea* spp. under no background flow conditions. Laboratory experiments on *Cassiopea* spp. under no background flow showed quantification of flow structures with peak velocities of 10 cm/s in the starting vortex; an increase in the fineness ratio during the power stroke; and a decrease in fineness ratio during the relaxation[33]. Pulsations of *Cassiopea* medusa primarily resulted in entraining ambient water in the radial direction (along the substrate) towards the bell and directing the entrained volume through its oral arms [33].

A numerical study examining the effects of bell pulsations and oral arms on exchange currents generated by *Cassiopea* spp. showed that the presence of oral arms increased the flux of flowing fluid from substrate to the bell [34]. Additional numerical studies on this model organism were conducted without background flow and with background flow to understand its suspension

feeding mechanism [35]. The presence of oral arms was suggested to aid suspension feeding process by providing resistance to the vortex structures generated during bell contraction [35]. The numerical model used in these investigations represented the oral arms as a homogenous porous layer.

Cassiopea spp. are mostly sessile, preferring to stay attached to the substrate and thus interact with permeable sediments. Previous experiments on permeable sediment layers showed the uptake of particulate matter by running water layers [36]. Also, laboratory experiments on agricultural sediments showed pore water uptake was achieved by running water [37]. These experiments showed that pore water uptake occurs due to forces acting on the sediments. One study conducted qualitative experiments with *Cassiopea* using colored sediment beds beneath the substrate, in order to verify if the bell pulsations could release the pore water [28]. The results showed that the dye was indeed released through the sand bed [28]. Thus *Cassiopea* bell pulsations can serve to release the pore water and mix it with the water column. An important limitation of this study was the results showing pore water pumping were entirely qualitative. Further, how pore water pumping of *Cassiopea* scales with bell size was not investigated.

While the previous experiments and numerical investigations commented on the importance of oral arms in trapping the vortices formed during bell pulsations and increasing the time scale for particulate water to stay, they were restricted to no background flow conditions. The natural environment of *Cassiopea* is dynamic with low (but finite) background flows. The first aim of this study improves upon the previous studies by examining how the organism-induced currents interact with the background flow. The second aim of this study provides quantitative characterization of pore water pumping by *Cassiopea*. To the best of our knowledge, both these aspects have not been examined in any previous study using *Cassiopea* medusa.

2.7 Pore Water Pumping

Several previous studies have examined pore water uptake by interaction of running water over sediments beds of varying topography. Experiments performed in wave tanks with water running over a sediment beds containing bromide showed an increase in bromide concentration in the overlying water. This increase was attributed to both molecular diffusion and advection introduced by running water [38]. Also, wave tank experiments using gravity waves over a sand substrate showed a fifty-fold increase in fluid exchange between the substrate and over lying water column when compared with only molecular diffusion [39]. This increase in pore water exchange was suggested to be due to the advection created by the waves over the substrate. It is here in expected that if there is a source of generating advective currents on a porous substrate, such as pulsations of *Cassiopea* individuals, then the pore water will be pumped through the substrate and mixed into the vertical water column. Quantification of this type of pore water pumping could be potentially useful in the bio-inspired design of unsteady pumps for biomedical applications. Further, the process by which these jellyfish are able to pump particles locked in the pores of the substrate vertically to the water column can be useful in designing engineering devices for use in applications such as cleaning oil spills, and removing algal blooms in ponds with mostly stagnant water. In this study, the pore water release by *Cassiopea* bell pulsations is characterized using Planar Laser Induced Fluorescence (PLIF) technique.

2.8 Engineering Applications of this Study

1. *Biomedical device design*. Recent investigations on membrane plasmapheresis comparing continuous and pulsatile blood flows showed that pulsatility enhanced plasma filtration, with reduction in hemolysis (rupture of blood vessel) [39]. In hemodialysis, blood from the body typically routed to a dialyzer using a series of intravenous, peristaltic pumps. The continuous flow aspect of these pumps increase time for the fluid transport. Unsteady pumps could potentially

minimize the time for blood to be transported outside the body and improve the overall efficiency of filtration process.

This study is expected to provide insight into particle capture under unsteady flow conditions, downstream use in developing filtration/separation devices for biomedical applications.

2. *Unsteady suction pumps for low Reynolds number applications.* The process by which *Cassiopea* jellyfish are able to remove particles trapped in the pores of the substrate can be useful in designing artificial suction pumps for use in applications such as removing oil particles from the sand in near shore regions following spills, and removing algal blooms in ponds with mostly stagnant water.

CHAPTER III

INTERACTION OF CASSIOPEA CURRENTS WITH BACKGROUND FLOWS

3.1 Introduction

A large number of sessile marine invertebrates such as sponges, gorgonians, brachiopods, polychaete tube worms, and bivalves use dome form of suspension feeding. Previous research on bivalves [4, 5] and sponges [6, 7], have characterized the steady currents generated by these organisms for suspension feeding. In addition to organism-induced currents, sessile invertebrates inhabiting the benthic boundary layer have to interact with ambient flows that may be continuous or oscillatory. Laboratory level experiments show that prey capture rates can be increased in oscillating flows when compared to the continuous flow conditions [8]. In terms of structural properties of feeding appendages, particle capture in colonies of flexible, sessile hydrozoans has been observed to depend mostly on the background flow velocity, colony reorientation and fluid resampling [8]. The flow velocity over a colony of flexible suspension feeders was observed to be dampened to increase the time scale available for suspension feeding [9]. Examining the diverse range of suspension feeding strategies used by sessile, benthic invertebrates could help in providing a broad understanding as to whether the choices of : (a) active (e.g., sponges) or passive (e.g., brachiopods) mechanisms; and (b) flexibleor mostly rigid feeding appendages, are potentially dictated by environmental flow conditions.

In contrast to the above studies, suspension feeding by sessile benthic invertebrates that generate unsteady currents has received limited attention. It can be expected that the physical mechanisms underlying suspension feeding using unsteady jets would differ from sessile invertebrates that either use continuous jets or feed in unsteady background flow conditions. We use the benthic *Cassiopea* jellyfish as a model organism in this study to examine how unsteady currents generated by organismal bell pulsations can impact suspension feeding

Cassiopea medusae, also known as "upside-down jellyfish" are found in patchy aggregations [13,24] in the benthic boundary layer of coastal environments such as mangrove swamps, coral reefs and seagrass meadows that are typically characterized by low ambient flows [25, 42, 43]. Population densities of 31 individuals m^{-2} have been observed in *Cassiopea* aggregations [29]**.** The morphology of *Cassiopea* includes an oblate bell with eight frilled, cylindrical oral arms containing numerous frilly branches (secondary mouths) fused over a central mouth [26]. These organisms exhibit a sessile life style, with their bell attached to the substrate and oral arms pointing towards the sunlight [27]. *Cassiopea* individuals rhythmically contract and expand their bell margins, entraining water adjacent to the substrate and generating vertical currents by directing the sampled water through their oral arms for suspension feeding. These organism-induced vertical currents help in minimizing recirculation of previously sampled water volume, while also providing the suction force necessary for the medusa to prevent dislodgement from the substrate.

Time-resolved and phase-averaged PIV measurements on *Cassiopea* individuals under no background flow have shown the formation f a starting vortex near the bell margin during the power stroke (bell expansion to contraction) of pulsations, with peak velocities on the order of 10 cm s^{-1} [33]. Kinematics analyses showed an increase in fineness ratio (bell height to bell diameter) during the power stroke and decrease in fineness ratio during the recovery stroke [33]. During *Cassiopea* bell pulsations, ambient water was entrained towards the medusa and passed through

the sieve formed by the oral arm network. A numerical study examining the currents generated by *Cassiopea* spp. under no background flow conditions showed that the presence of oral arms increased the volumetric flux [34]. Additional numerical studies on this organism without background flow and with background flow were conducted to understand its prey capture mechanism. The results of these studies were used to propose that the oral arms play an important role in suspension feeding, by trapping the vortices formed during the pulsations and increasing prey retention time [24].

These numerical models were limited to 2D representation of the bell pulsations, which was attributed as one of the reasons for disagreement with the experimental data on *Cassiopea* individuals in the far-field flow above the medusa. Further, the oral arms were approximated as a homogenous porous layer in the numerical studies. Finally, though the natural environment of *Cassiopea* characterized by low–speed background flows on the order of a few centimeters per second, the interactions of organism-induced currents with non-zero background flows was not examined in any of the above studies.

In this study, we focus on examining the hydrodynamic interactions of *Cassiopea* pulsation-induced jets with continuous background flows. Multiple *Cassiopea* individuals were used for this study to examine how flow characteristics change with bell diameter and pulsing frequency. The animals were tested in a recirculating laboratory flow tank under varying background flows ranging from 0-2 cm/s. 2D videos were used to quantify bell pulsation kinematics. 2D time–resolved PIV measurements were obtained to visualize the formation of flow structures near the bell margin and interactions with background flow. 2D time-averaged PIV measurements were used to quantify bulk flow characteristics of variable medusa size on background flow and implications for suspension feeding.

3.2 Materials and Methods

3.2.1 *Cassiopea* spp. collection and handling

Cassiopea individuals of varying bell sizes were obtained from Carolina biological supply, NC, USA, during May 2016. Five individuals were used in this study with bell diameters ranging between 2 cm to 7 cm. The medusae were transported overnight and placed in a 20-gallon glass aquarium maintained at 20-24^{o}C with artificial salt water with salinity 1.024 g L^{-1}. The medusae were target fed live *Artemia* spp. nauplii for every two days. Metal halide lighting was used in the 20-gallon tank used for housing the medusa, and set to operate between 8-10 hours continuously on a daily basis. Submersible heaters were used to ensure the housing tank water was maintained at a temperature range of 20-24^{o}C. All experiments were conducted at room temperature during summer of 2016 (May to July).

3.2.2 Low speed recirculating flow tank

Fig. 5, represents the recirculating flow tank that was designed in the same manner as outlined by Vogel and LaBarbera [44]. The fabricated flow tank was capable of producing low-speed, continuous background flows on the order of 1 cm s^{-1}. Flows with mean velocities in the range of 0 - 2 cm s^{-1} were produced with a universal DC motor **(**1/3 hp, 1800 rpm, AutomationDirect**,** GA, USA) regulated with a variable speed DC controller with 50:1 speed reduction (Dart Controls, Inc., IN, USA). In addition, a custom gearbox with 250:1 speed reduction and 10:1 pulleys connected to commercial timing belts were both 3D printed and assembled with the motor shaft for the multiple orders of magnitude speed reduction necessary for this study. The Dc motor drove a 3D printed, 3-bladed propeller (with fixed stator blades) that was positioned vertically inside the return piping following the test section exit. Rotation of the propeller drove the flow through the test section. The test section was 1 ft x 1 ft in cross-section and 3 feet long when measured between two custom flow straighteners. The entire test section was made from 1-inch

acrylic sheets for optical accessibility. Flow straighteners were used at the entrance and exit of the test section to generate uniform flow across the observation window used in this study. A sand bed was made using commercially available black substrate (CarbSea Tahitian Moon reef &Marine Substrate, CaribSea Inc., FL, USA) with 0.1-0.3 mm grain diameter. A substrate depth of 2-inches was used for qualitative flow visualization tests, while 1-inch depth substrate was used for all PIV measurements. Artificially made 100-gallons of de-ionized water with 1.025 g/L was prepared using aquarium sea salt (Instant Ocean Spectrum Brands, VA, USA) and used to fill the recirculating flow tank.

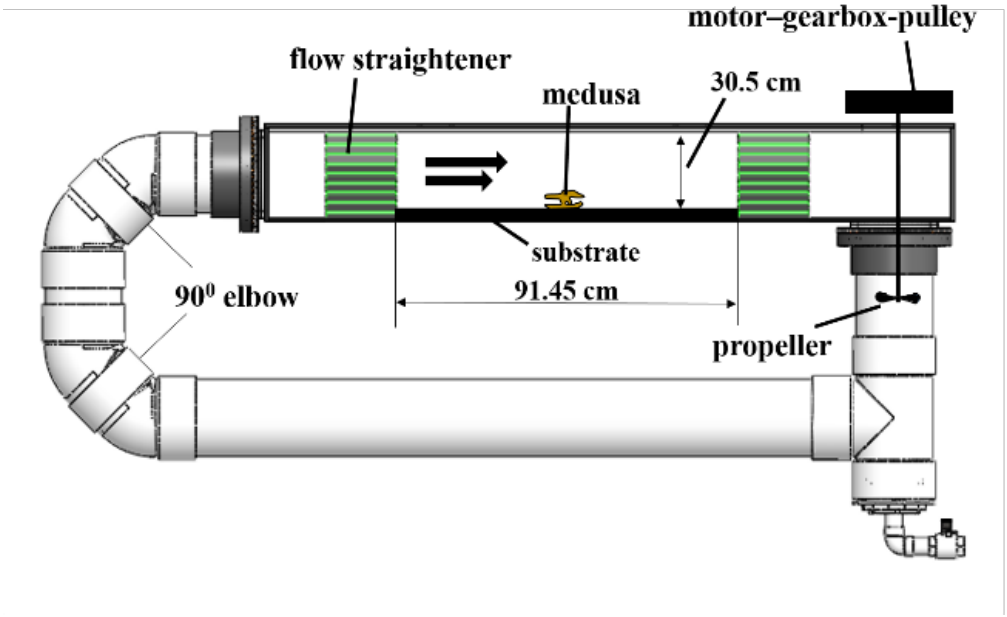

Figure 5. Schematic diagram (not to scale) of recirculating flow tank used to introduce background flows on *Cassiopea* individuals. The medusa was positioned in between two flow straighteners as shown. Individual animals were placed on top of the sand bed.

3.2.3 Bell kinematics

Bell kinematics experiments were conducted on *Cassiopea* individuals placed inside a 3 gallon cubic plastic aquarium with dimensions of 12.7 cm x 12. 7 cm x 12 cm. Video recordings were obtained using a digital camera (EOS70D, Canon Inc., Japan) with a maximum spatial resolution of 1,920 x 1,080 pixels. All videos for bell kinematics analyses were acquired using 60 mm focal

lens at a frame rate of 30 Hz. A dark background and black sand were used to provide additional contrast between the medusa and its surroundings. Each medusa was moved into the tank after verifying the water conditions were closely matched to the 20-gallon aquarium used for housing the animals. The following conditions were matched between the test and housing aquaria: pH, salinity, temperature, ammonia, nitrate and nitrite. Each medusa was drip-acclimated into the test aquarium and a half-day resting period was provided for every individual to settle on the substrate. After 12 hours, a plastic ruler was placed above the substrate, bisecting the central plane of medusa bell and perpendicular to the camera image. The camera was focused to obtain nearly uniform illumination across the image planes. A still image of the ruler was acquired for scaling from pixels to cm. The experimental recordings consisted of a minimum 10 continuous bell pulsation cycles. The recorded images were digitized and processed using MATLAB DLTdv5 program [45]. Eight points were digitally selected on one side of bell margin and one point on the oral arm (Fig. 6), and these points were tracked manually across 10 continuous pulsing cycles. Instantaneous fineness ratio F_i, defined as ratio of bell height h to bell diameter d at each particular instant was obtained from the digitized images. Eight points on bell were used to quantify bell motion and one point on the oral arm was used to examine its movement with respect to the bell. Reference points were placed only on half of the bell diameter assuming radial symmetry and were investigated.

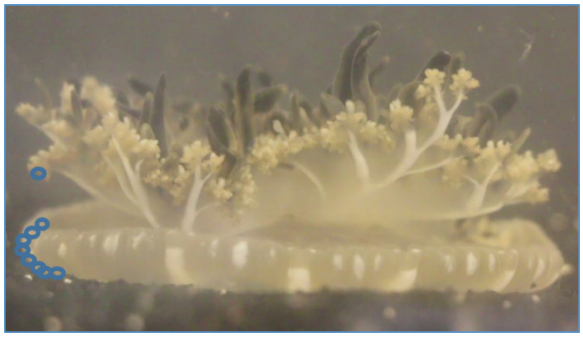

Figure 6. Representative image of bell kinematics with eight markers on bell margin and a single marker on distal end of oral arm.

3.2.4 Qualitative flow visualization

A single, *Cassiopea* individual with bell diameter d = 4 cm was placed in the recirculating flow tank with a sand bed of 2-inch height, after verifying the water conditions with the main tank, including salinity, temperature and the previously mentioned chemical conditions. 5 ml of organic red food color (McCormick & Co., Inc., MD, USA) was added to 1 L of de-ionized water and was filled into a micro-pipette. The micro-pipette tip was positioned just above the substrate adjacent to the medusa, in the upstream position (approximately 2d to the left of the medusa, observed in the camera view), such that ejected dye would flow along the central plane of organism (Fig 7). The dye was injected into the water when the medusa started pulsing, for visualizing the flow structures generated by interaction of pulsation-induced currents with the background flow. For these tests, background flow ranging from 0 - 2 cm s^{-1} was used. Videos were recorded using at a frame rate of 30 Hz using the same camera used for bell kinematics measurements (EOS70D, Canon Inc., Japan).

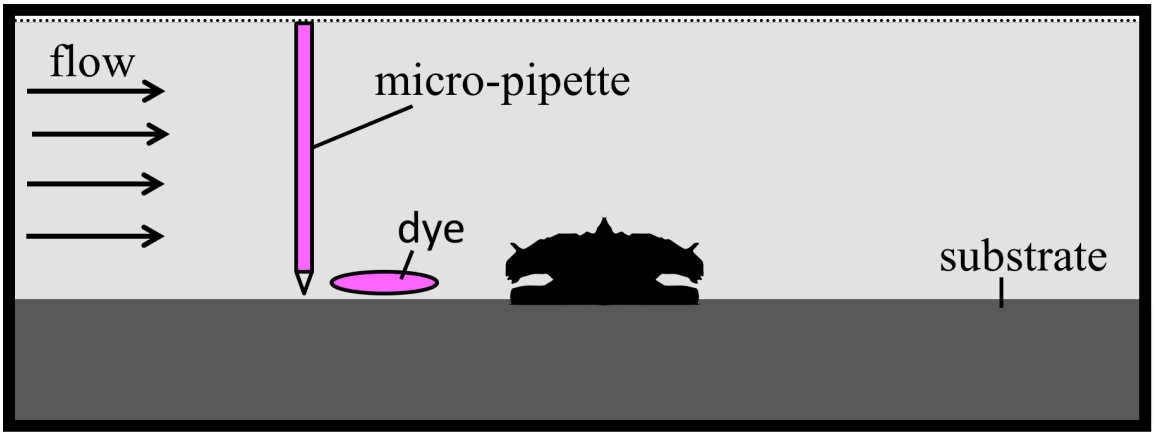

Figure 7. Flow visualization experimental setup. Dye was fed from a micro-pipette adjacent to the substrate of 2 in depth and upstream of the medusa.

3.2.5 2D Time-resolved particle image velocimetry (PIV)

Experimental setup for PIV is shown in Fig. 8. 2d time-resolved PIV was performed on an individual medusa with 2 cm bell diameter. High-speed videos were recorded with 1 megapixel CMOS camera (Phantom Miro 110, Vision Research Inc., Wayne, NJ, USA) at frame rate of 696 Hz using a 60mm constant focal length lens (Nikon Micro Nikkor, Nikon Corporation, Tokyo, Japan). The maximum spatial resolution of the camera (1280 x 800 pixels) was used for recording. Two background flows of mean velocities 0.45 cm s^{-1} and 2 cm s^{-1} were considered for this set of experiments. The field-of-view (FOV) used was ± 1.5 d measured from the center of the medusa. The flow field was illuminated using a 0.5 mm diameter beam outputted by a 35mJ high-speed, single cavity Nd:YLF laser (Photonics Industry Inc., NY, USA) with wavelength 527 nm. The beam was converted into a planar sheet of 3 mm thickness using a cylindrical lens (focal length = 20 mm). The laser sheet was positioned to be perpendicular to the substrate along the diameter of medusa as shown in Fig. 3. Hollow glass spheres of 8 – 10 μm) diameter (LaVision GmbH, Gottingen, Germany) were used as seeding particles. Small amounts of these seeding particles were mixed in with water from the flow tank in a 1000 mL beaker before being added into the tank. This process was repeated with the water recirculating until uniform particle

seeding density in the range of 10-20 particles for 5-10 pixels/particle was obtained and particle displacements in the range of 4-7 pixels was measured between two successive images. Both the Nd: YLF laser and the camera were connected to high speed controller. This controller was then connected to a central computer that was used for image acquisition. The recordings used for this study did not commence until after the flow tank was continuously operating for at least 1-hour, so as to allow time for uniformly mixing the seeding particles and also to provide a short period for the medusa to adjust to their new environment.

For each 2D time-resolved PIV run, 100 images were acquired to obtain atleast one complete pulsation (both power stroke and the recovery stroke). Five test runs for each medusa for all background flows were recorded to obtain five complete pulsing cycles and processed to obtain 2D velocity vector fields. The raw images were processed using multi-pass cross correlation in DaVIS 8.2.0 software (LaVision GmbH, Gottingen, Germany). The interrogation window sizes used were 96 x 96 pixels with 50% overlap (2 passes) and 48 x 48 pixels with 50% overlap (2 passes). Post-processing was performed by rejecting velocity vectors with peak ratio of less than 1.2 and interpolating the empty vectors. The processed data were exported into .dat file format, where each file consisted of spatial coordinates (x, y) and corresponding 2D velocity components (horizontal component u in x-direction and vertical component v in y-direction). Images corresponding to each phase percentage in all test runs were exported as ".dat" files and were then phase-averaged using MATLAB (The Mathworks, Inc., Natick, MA) program to get single .dat file containing vertical co-ordinate y, horizontal co-ordinate x, vertical velocity component v, horizontal velocity component u, and 2D velocity magnitude V. This .dat file was then processed in TecPlot360 (Tecplot Inc., WA, USA) to get time-resolved 2D PIV results.

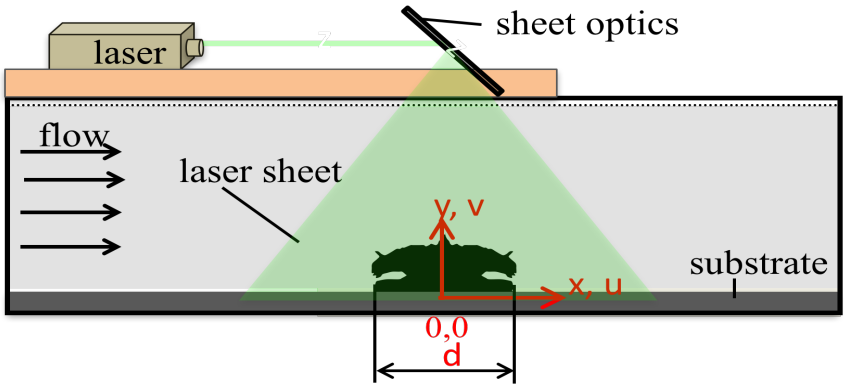

Figure 8. Experimental setup used for 2d PIV measurements (time-resolved and time-averaged). The coordinate system origin is defined at the center of medusa. Horizontal velocity component (u) is defined along x-axis, vertical velocity component (v) is defined along y-axis and d is bell diameter in mm.

3.2.6 2D Time-averaged PIV

2D time-averaged PIV measurements were conducted to quantify bulk flow characteristics across multiple medusae of different sizes under varying background flows. Experimental setup used was the same as that of 2D time-resolved PIV, except that images were acquired using an sCMOS camera (LaVision GmbH, Gottingen, Germany) with full resolution of 2600 x 2200 pixels in double-frame mode. Laser pulse separation times (time between two images in an image pair) ranged from 10-20 ms, depending on the magnitude of background flow. Frame rate of 15 Hz was used for time-averaged PIV recordings, with a field of view of ± 1.5 d. Particle displacements between two images in an image pair were ensured to not exceed 25% of the smallest interrogation window size (8 pixels). Fourteen pulsation cycles under each background flow were recorded and processed using multi-pass cross-correlation in DaVIS 8.2.0 software (LaVision GmbH, Gottingen, Germany). The interrogation window sizes included 64 x 64 pixels with 50% overlap and 32 x 32 with 50% overlap (2 passes each). Post-processing was performed by rejecting velocity vectors with peak ratio of less than 1.2 and interpolating the empty vectors. Following post-processing, time averaging was performed in DaVIS 8.2.0 software to result in a

single 2D velocity vector field. The time averaged image was exported in .dat file format containing 2D spatial coordinates (x, y) and 2D velocity components (horizontal component u and vertical component v) and imported to TecPlot360 (Tecplot Inc., WA, USA) for extracting velocity profiles. A custom program, written in MATLAB (The Mathworks, Inc., Natick, MA), was used to calculate volumetric flux upstream and downstream of the medusa.

3.3 Results

3.3.1 Bell kinematics

Temporal patterns of bell pulsations were manually analyzed from the recorded frames to evaluate durations of the power stroke, recovery stroke, and the complete cycle. Each cycle was divided into two parts of 0% to 100%, with 20% increment, consisting of power stroke and recovery stroke frame number. Power stroke time and recovery stroke time for each cycle for an individual *Cassiopea* was calculated by the difference of 0% and 100% divided by the recording frame rate of 30 frames s^{-1}. Fig. 9 shows the pulsing frequency variations across the individual medusae used in the experiments and across all background flows (0 cm s^{-1}, 0.45 cm s^{-1} and 2 cm s^{-1}). Pulsing frequency increased for bell diameter d =3 cm from d= 2 cm and later decreased with increase in bell diameters from 4 cm through 7 cm. Standard deviation was calculated based on variable background flow for each medusa.

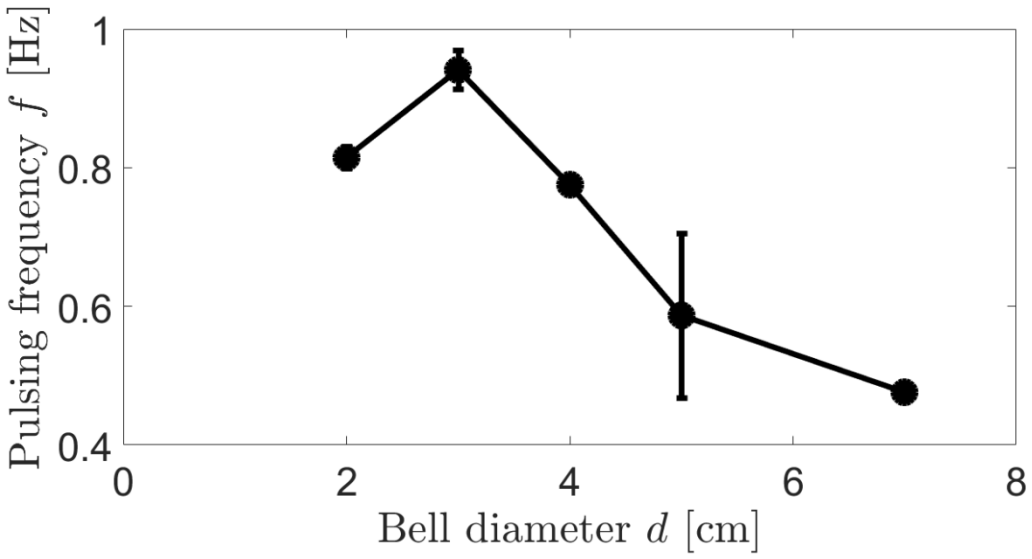

Figure 9. Plot shows variations of pulsing frequency with standard deviations for each medusa under variable background flows (0 cm s^{-1}, 0.45 cm s^{-1} and 2 cm s^{-1}).

The instantaneous fineness ratios for the bell and the arm were analyzed for *Cassiopea* individuals with bell diameters of 2 cm, 3 cm, and 4 cm respectively. Bell motion was inward (towards the center) during the power stroke. During the recovery stroke, the bell moved outwards and downward towards substrate.

The bell kinematics conducted on the three different size medusae were observed under no background flow. The kinematics result shown in Fig. 10A is in agreement with previous observations [33] such that during the contraction phase, the diameter of all three medusae decreased resulting in an increase in the fineness ratio. During the recovery stroke, the bell diameter increased and the fineness ratio decreased. The bell fineness ratio remained constant for most of the recovery stroke, followed by a sharp increase during the power stroke.

The 2 cm and 4 cm individuals had longer oral arms compared to their bell diameters, and therefore, their respective plots show the arms overlapping the bell as shown in Fig. 10B. The 3 cm *Cassiopea* had smaller oral arms and thus showed little variation.

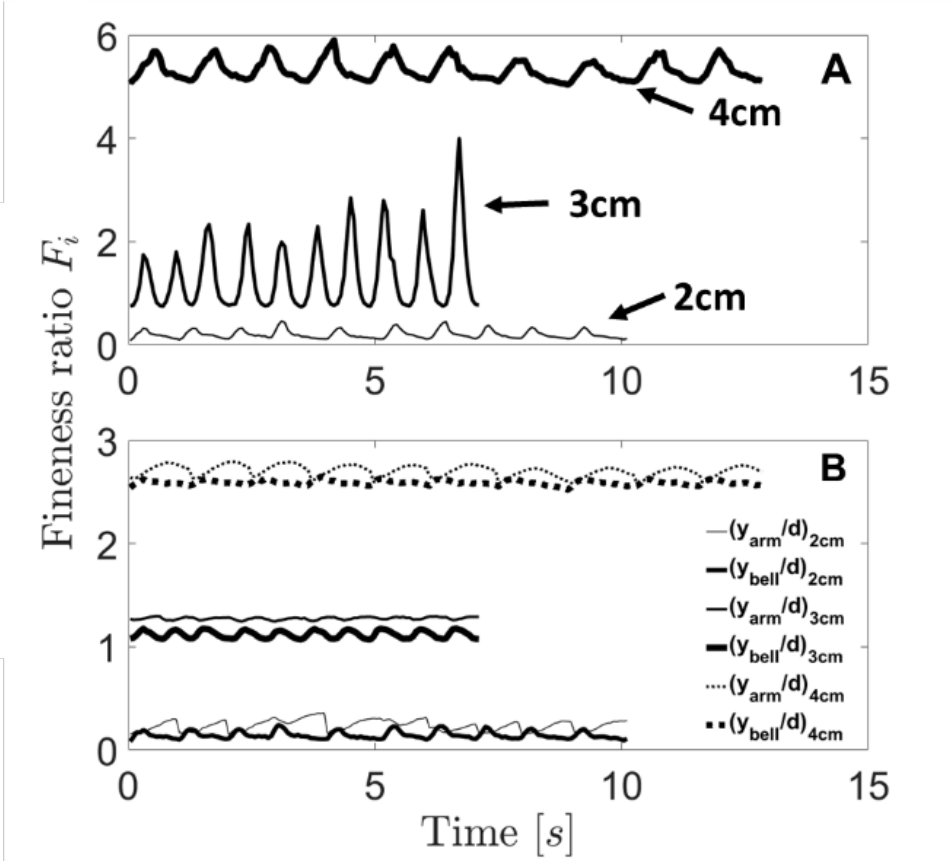

Figure 10. Instantaneous fineness ratio vs time for three medusae with bell diameters 2 cm, 3 cm and 4 cm. F_i was calculated as the ratio of the bell height h to the bell diameter d. (B) Bell fineness ratio defined as the axial position of the tip of the bell divided with the bell diameter vs time are plotted. Data were acquired from three medusae with bell diameter (d) 2 cm, 3 cm and 4 cm. Profiles show variation in time over 10 pulsing cycles. Each cycle consists of 10 data points. Data for 3 cm and 4 cm are offset from 2 cm with 1 and 5 units respectively for instantaneous fineness ratio and also 1 and 2.5 respectively for bell and arm fineness ratio.

3.3.2 Qualitative flow visualization

Under no background flow conditions, colored dye released from the micro-pipette was entrained into the subumbrellar cavity of the medusa during the contraction phase of bell pulsation. This resulted in the formation of a starting vortex adjacent to bell margin which was directed toward the oral arms during the recovery stroke. The elaborate network of the oral arms provides resistance to the flow, breaking up the coherent starting vortex into small–scale flow structures.

These small-scale flow structures were introduced into the water column in the form of a vertical jet as shown in Fig. 11A. The change in dye coloration near the substrate and above the oral arms suggests that the oral arms diffused the dye by slowing down the jet. The small-scale flow structures were less diffuse under non-zero background flow as shown in Fig. 11B.

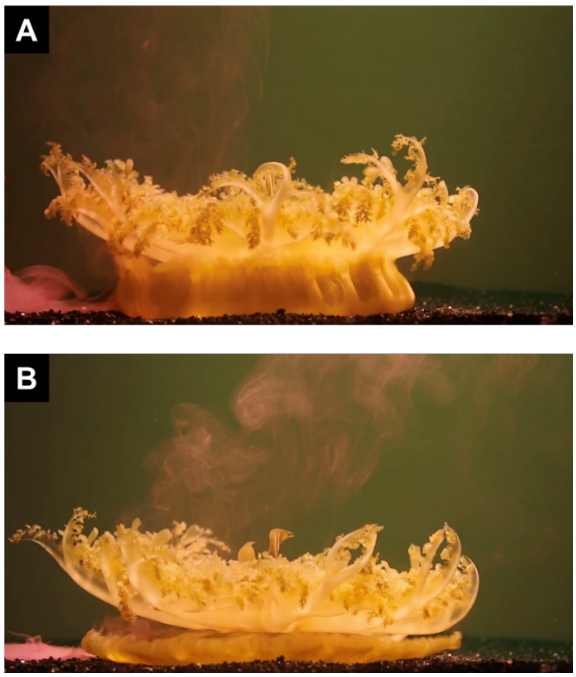

Figure 11. Qualitative flow visualization of *Cassiopea* currents. Individual medusa of bell diameter d =9 cm was tested under(A) no background flow and (B) background flow 2 cm s^{-1} conditions. The interaction of the organism-induced jet with the background flow can be visualized via the diffusion of dye in the water column.

3.3.3 Time-resolved flow characteristics

3.3.3.1 Power stroke

Phase-averaged velocity vector fields were examined for a 2 cm medusa under background flows of 0.45 cm s^{-1} and 2 cm s^{-1}. Fig. 12 shows the flow fields at specific instances of power stroke for

2 cm medusa under 0.45 cm s^{-1} background flow. At 20% PS, the water around the individual was pulled towards bell margin along the substrate with 0.3 cm s^{-1} as shown in Fig. 12A. At 60% PS starting vortex formation was observed and fluid velocity at bell margin was increased to 0.6 cm s^{-1} as shown in Fig. 12B. Further into the pulsing cycle, this vortex was carried along the bell margin and was directed vertically through the oral arms. The velocity of current induced into background flow was around 0.35 cm s^{-1}. The leading vortex (upstream end of bell margin) formed was smaller compared to the trailing vortex (downstream end of bell margin), due to diminishing influence of background flow with increasing downstream distance.

A similar pattern was observed in power stroke of the same 2 cm individual when background flow was increased to 2 cm s^{-1} as shown in Fig. 13A-C. When the background flow increased the vortex with velocity vectors of 0.5 cm s^{-1} in downstream bell margin location was observed while a smaller vortex formation was observed in upstream bell margin point as shown in Fig. 13C. This was due to interaction of the background flow on the vortex structure.

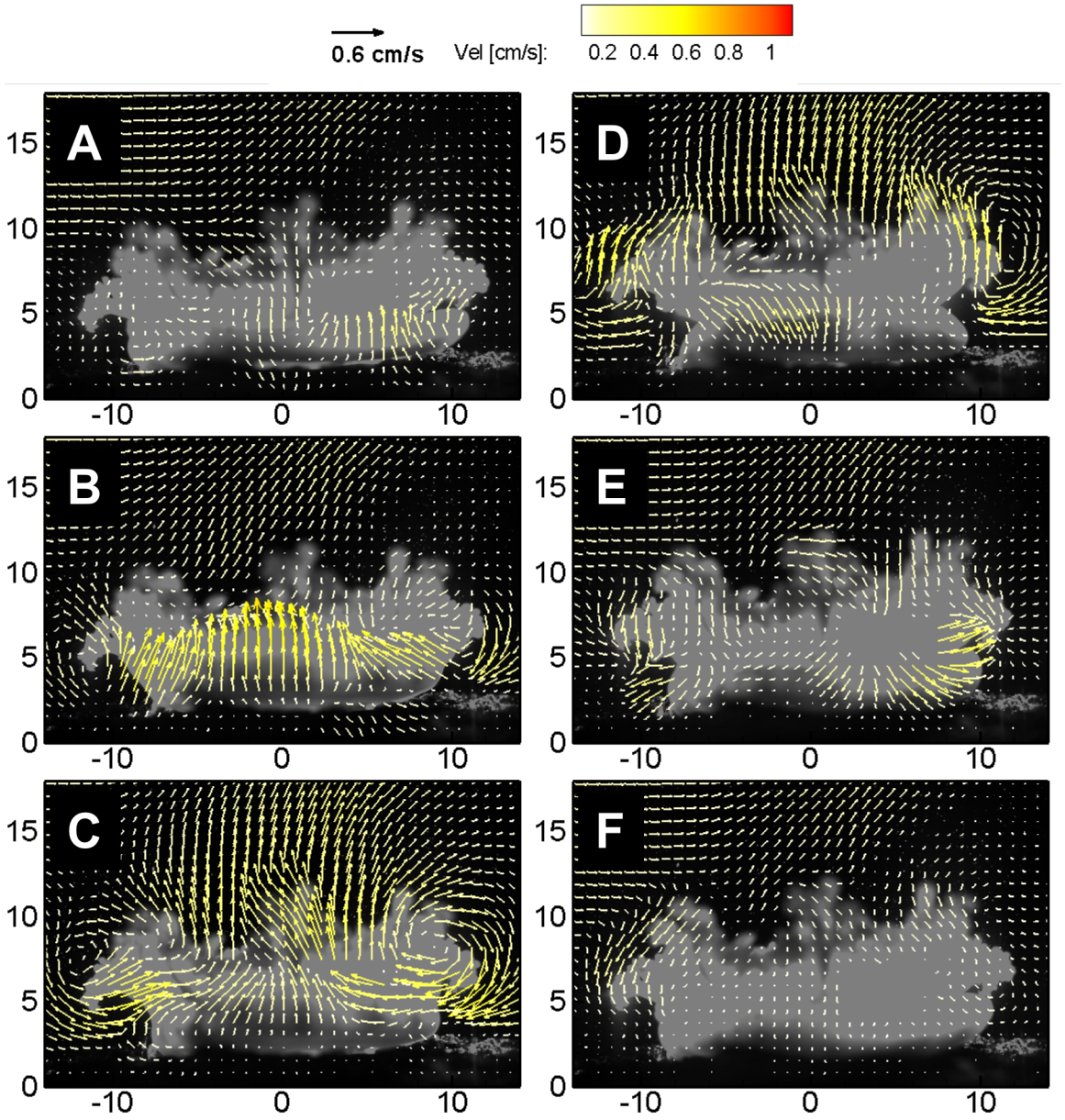

Figure 12. Time resolved velocity vector field images of 2 cm *Cassiopea* medusa with background flow of 0.45 cm s^{-1}. (A) Power stroke 20%, (B) 60% of power stroke, (C) 100% of power stroke, (D) 20% of recovery stroke, (E) 60% of recovery stoke and (F) 100% of recovery stroke. Length of vectors represent their magnitude as shown in legend and direction indicates the flow direction.

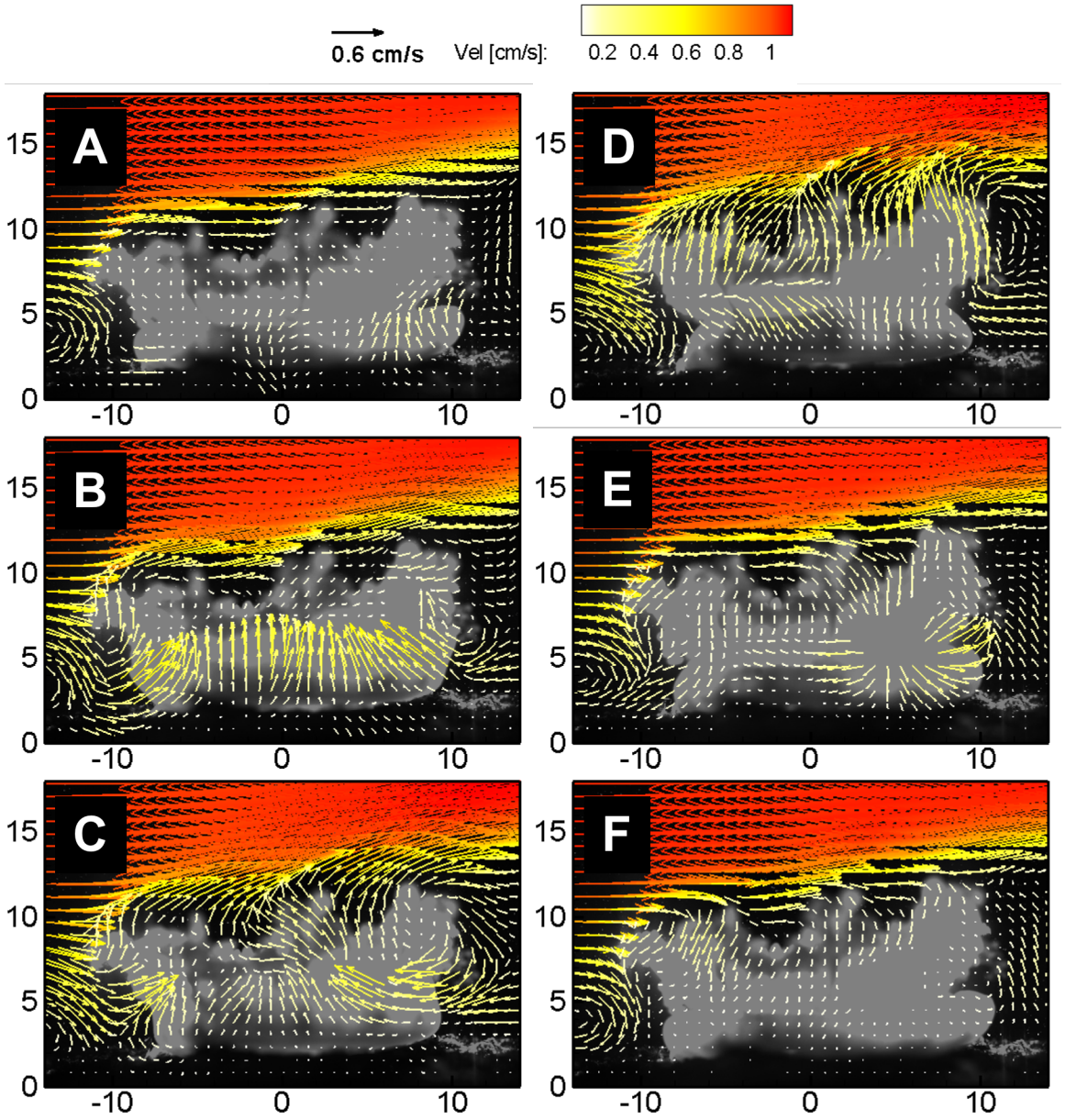

Figure 13.Time resolved velocity vector field images of 2 cm *Cassiopea* medusa with background flow of 2 cm s^{-1}. (A) Power stroke 20%, (B) 60% of power stroke, (C) 100% of power stroke, (D) 20% of recovery stroke, (E) 60% of recovery stoke and (F) 100% of recovery stroke. Length of vectors represent their magnitude and direction indicates the flow direction.

3.3.3.2 Recovery Stroke

On observation of recovery stroke vector field time resolved images, vortex was advected upward at 20% RS as shown in Fig. 12D. This vortex diminished as the recovery stroke progress. At 60% RS, water started to expel out with 0.3 cm s^{-1} into upstream and 0.4 cm s^{-1} in downstream as shown in Fig. 12E. The water present inside sub-umbrella region was appeared to expel out as recovery stroke progressed. At the end of recovery stroke, 100% RS, no significant water movement was observed in the downstream direction, as shown in Fig. 12F.

As the background flow increased to 2 cm s^{-1}, the velocity vectors in vortex decreased in upstream side during 20% RS as shown in Fig. 13D while the velocity value was approximately same in downstream side. Vortex was advected into water column and velocity vectors in vortex were approximately 0.3 cm s^{-1}. As recovery stroke progressed, on downstream of medusa water started to expel out as shown in Fig. 13E. At end of 100% RS no flow was observed on downstream but vortex similar to vortex was observed on upstream near bell margin as shown in Fig. 13F. Asymmetry in vortices advection was observed due to increased background flow.

3.3.4 Cycle-averaged flow characteristics

3.3.4.1 Velocity profiles

For a particular medusa, as the background flow increases from 0 cm s^{-1} to 2 cm s^{-1}, the horizontal velocity component u at various locations along substrate were plotted against the vertical column height as shown in Fig. 14A. Decrease in horizontal velocity component u can be observed at x = d and 1.5 d. This decrease in horizontal component u was due to interaction of medusa jet with the background flow. Also the interaction of the medusa jet on the background flow can be seen in the vertical direction at a distance 2d in the downstream.

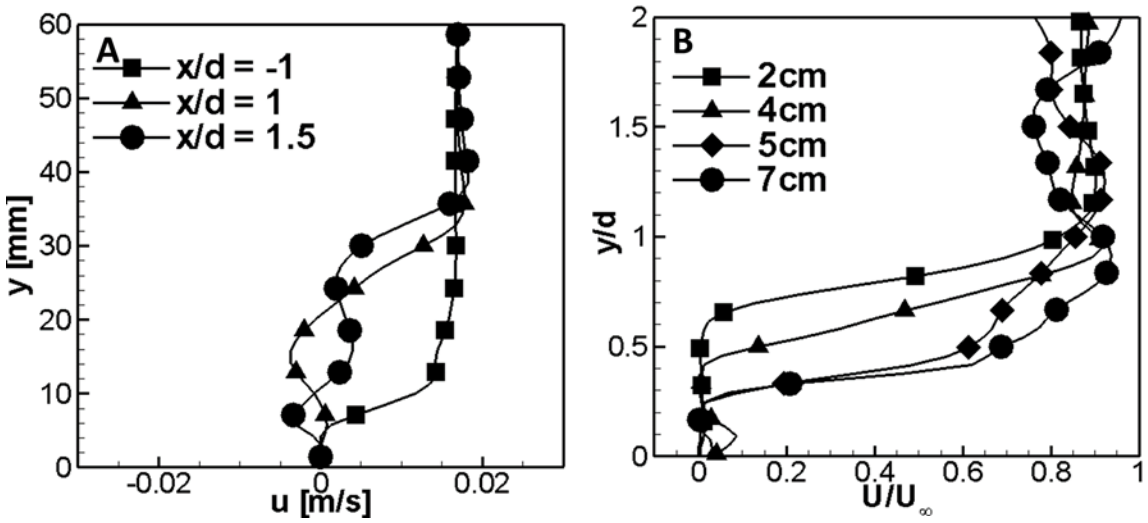

Figure 14. (A) Horizontal velocity component (u) was plotted against vertical height for 2 cm medusa at various positions along the substrate with background flow of 2 cm s^{-1}. (B) Non-dimensional centerline velocity, ratio of centerline velocity (U) to ambient background flow velocity (U_∞ = 2 cm s^{-1}), was plotted against jet penetration along vertical height for various medusae with bell diameters 2 cm, 4 cm, 5 cm and 7 cm.

Non-dimensional centerline velocity U/U_∞ vs jet penetration ratio, defined as ratio of vertical column height y to bell diameter d, for various medusae were plotted in Fig. 14B. Non-dimensional centerline velocity U/U_∞ is ratio of medusa jet centerline velocity to ambient background flow velocity i.e. 2 cm s^{-1}. From Fig. 14B, the jet penetration ratio y/d for a given U/U_∞ value looks larger for medusa with d = 2 cm. This figure also shows that at particular U/U_∞, jet penetration ratio decreased with increase in medusa bell diameter d. This decrease in penetration was due to the decrease in pulsation frequency with diameter from Fig. 9. Thus an inverse proportionality relationship exists between jet penetration ratio and non-dimensional centerline velocity. We can observe the centerline velocity U of all medusa reached 90% of ambient velocity U_∞ at y = d. We can conclude the medusa jet affects the background flow for 1 d radially along the medusa central axis and in the downstream.

3.3.4.2 Volumetric flux

Instantaneous volumetric flux was calculated at x/d = -1, 1 and 1.5for 14 pulsing cycles for 2 d vertically at each location. Fig. 15A shows sample location of x/d = -1(triangle markers), x/d = 1 (circle markers) and x/d = 1.5(diamond markers) for medusa d= 4 cm for 2 d vertically. It was then averaged to get mean volumetric flux $\bar{Q}$. Absolute value of this mean volumetric flux was obtained for various medusae and graph was plotted against bell diameter with background flow of 2 cm s^{-1} as shown in Fig. 15B. With increase in diameter, the absolute mean volumetric flux increased. Also, mean volumetric flux is less in downstream locations of x/d =1 and 1.5 compared with upstream location x/d = -1. This decrease in volumetric flux was due to medusa current interaction with the background flow, and also the form drag created due to oral arms of individuals. To look at the effect of medusa current interaction with background flow, the medusa flow field in no background flow was subtracted from background flow conditions as shown in Fig 15C-D. Fig 15 C shows the subtraction of velocity vector field with no background flow condition from 2 cm s^{-1} background flow for smaller medusa of diameter 2 cm. While Fig 15 D shows the subtraction of velocity vector field with no background flow condition from 2 cm/s velocity vector field of larger medusa of 7cm bell diameter. The vector field show the influence of smaller medusa current up to 2d while the effect of 7 cm medusa pulsation was found up to 1.5 d in vertical direction.

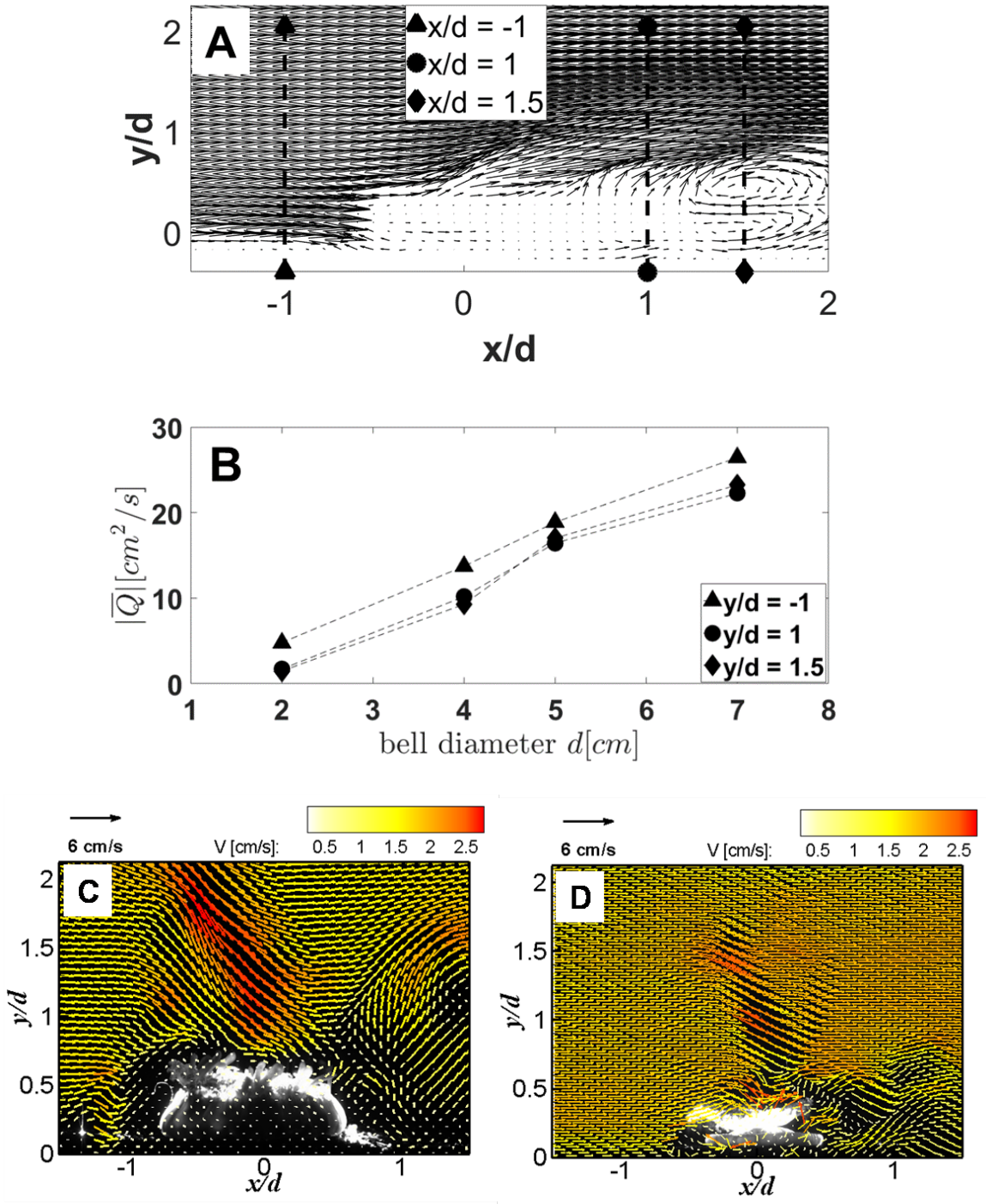

Figure 15. (A) Plot shows locations x/d= -1(triangle markers); x/d= 1 (circle markers) and x/d = 1.5 (diamond markers) used for calculating volumetric flux in background flow of 2 cm/s. (B) Absolute mean volumetric flux was plotted for medusa with bell diameter 2 cm, 4 cm, 5 cm and 7 cm with background flow. Absolute mean volumetric flux decreased in downstream locations compared to upstream location. Subtracted no flow fields condition from 2 cm/s flow field condition for (C) smaller medusa d= 2cm and (D) larger medusa d= 7 cm.

3.4 Discussion

Phase averaged time resolved velocity vector fields showed flow with peak velocities around 0.3 cm s^{-1} were generated during starting vortex formation in the power stroke. This starting vortex was pushed through the oral arms in the manner of a high-shear flow with magnitude roughly 0.3 cm s^{-1}. This value of peak velocities of the organismal currents remained same in both background flow conditions 0.45 cm s^{-1} and 2 cm s^{-1}. Thus when the background flow increases, the flow affects the medusa current and vice versa. The velocity vectors magnitude was slightly decreased in the upstream stream due to direct interaction of background flow while in downstream, no significant changes were observed. Lack of change in velocity magnitudes downstream of the medusa was primarily due to the resistance or drag created by the individual bell pulsations. These results resemble engineering studies of jets in cross flow [46] such as formation of asymmetric vortex rings. Thus more particulate matter can be entrained by suspension feeding *Cassiopea* on the downstream side as compared to the upstream side, enabling time scales necessary for increasing capture and retention rates.

2D time-averaged far-field data showed decrease in velocities with increase in downstream location for each bell diameter. Also calculations of centerline jet penetration for a background flow of 2 cm s^{-1} showed an inverse relationship between bell diameter and the corresponding centerline velocities. This decrease in penetration height with increase in bell diameter is most likely caused by the decrease in pulsing frequency. Due to more frequent pulsations by smaller medusa, a larger cumulative effect can be realized via introducing vortices from multiple cycles into the background flow. Additionally, smaller medusa can generate more shear flow due to faster time scales of bell pulsation. Finally, qualitative flow visualization showed the breakup of large-scale vortices into small-scale flow structures due to passage of flow generated in power stroke through the oral arms. This indicates that high resistance imposed by the oral arms plays a critical role in enhancing the suspension feeding mechanism, with or without background flow.

Absolute mean volumetric flux was calculated with 2 cm s^{-1} background flow conditions to understand the flow entrainment along the medusa current. The smaller individuals had larger jet penetration, creating larger deceleration zone downstream and increasing time scale for sampling necessary for suspension feeding. In the case of large medusae, the absolute mean volumetric flux was increased showing a larger deceleration zone downstream of the organism when compared to smaller medusa. Such a large deceleration zone could be produced due to larger surface area and consequently larger form drag. This decelerated zone increases the time scale for suspension feeding, similar to what was described earlier for smaller individuals. The fundamental difference is the elevated role of oral arm and body morphology in the case of larger medusa, whereas the faster rate of pulsations in smaller medusa results in increased jet penetration into background flow. Thus, individuals could alter their jet velocity by modulating their pulsing frequency based on the background flows, so as to increase the time scale for suspension feeding as shown in Fig 16.

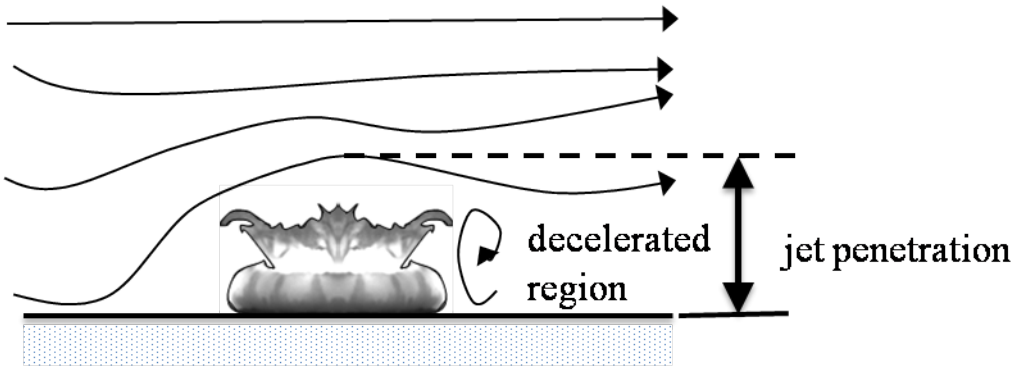

Figure 16. Formation of decelerated zone in the downstream of medusa. For small medusa, decelerated zone was formed due shear caused by its jet penetration in cross flow. For large medusa, the decelerated zone was formed due to form drag.

Particle capture by *Cassiopea* was not visualized or measured in this study. Measurements of *Cassiopea* feeding and retention rates are needed to understand the role of asymmetric vortex ring formation beneath the oral arms under non-zero background flow conditions. As these medusa live in fairly larger aggregations, it would be necessary to examine how individuals in a group

interact when in close proximity of each other. This is especially necessary under non-zero background flow conditions. Previous experiments on corals showed that particle capture increased with increase in the number of neighbors under high background flow conditions, and decreased with increase in neighbors at low background flow conditions [47]. Pressure drop of 0.1 mm to 0.4 mm H_2O was found in sponges, cnidarians according to modern retention theory [48]. Since corals and *Cassiopea* spp. have same pressure drop range, whether *Cassiopea* would follow the same trend of particle retention as corals must be investigated. Though *Cassiopea* stays in patchy aggregations, it is unclear if there are synergistic interactions between neighbors. Modulating the pulsing frequencies based on nearest neighboring medusae as well as the background flow provides multiple pathways to tailor an individual's pulsations to maximize feeding success.

3.5 Conclusions

This paper provided details on how background flows interacts with the currents induced by *Cassiopea* medusa. *Cassiopea* pulsations locally alters the flow field up to horizontal distance of around one diameter downstream from the medusa center. The cross flow interaction with the upstream end of the bell margin resulted in an asymmetric starting vortex. Along the oral-aboral axis, the background flow reached 95% of its velocity at one diameter vertically measured from the substrate. The volumetric flux downstream of the medusa decreased when compared to upstream position, due to the organism-induced jet interaction with background flow. The implications of the observed flow fields on suspension feeding was discussed.

CHAPTER IV

PORE WATER PUMPING BY CASSIOPEA INDIVIDUALS

4.1 Introduction

Movement of water in the benthic boundary layer is negligible compared to free stream water. In order to obtain food, living organisms such as *Cassiopea* medusa, tapeworms etc., pulsate continuously. The pulsations of *Cassiopea* helps in exchanging fluids with surrounding to maintain the ecology and to support their life.

Cassiopea medusa pulsate their bells creating vortex structure around along bell margin. These structures help in entrainment of prey particles present around the organism. This captured water sample is then pushed through its oral arms as a current, while the prey is captured on the oral arms by sieving technique. During the pulsing mechanism, along with food capturing process there is also entrainment of pore water containing dissolved organic and inorganic matter present beneath substrates [28]. This dissolved organic and inorganic matter are required for the other predators [28].

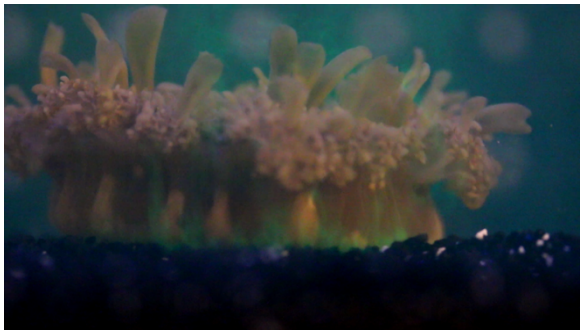

Figure 17. Qualitative visualization of pore water entrainment. Release of fluorescence can be observed near the bell and substrate interface.

Previous experiments with colored substrates showed enhancement of color into water column [38, 34] as shown in Fig 17. But quantitative information of such pore water enhancement is not available. Here we use PLIF technique to quantify the pore water enhancement using [49], where the concentration at each pixel can be calculated using:

$$C(i,j) = \text{mean}(B_n\text{-}D)*(I_n\text{-}B_n)/(\alpha a*(B_n\text{-}D)$$

Where B_n is background image intensity, D is dark image intensity, I_n- unknown image intensity that need to be calculated for concentration, α is proportionality constant between concentration and intensity, a is attenuation coefficient.

So to non-dimensionalize the concentration at each pixel, maximum available concentration at each instant. If C is concentration of organic/ chemical component at each pixel obtained after equation 1, C_{max} is maximum concentration of organic/chemical component at an instant then due to the effect of pulsations, the concentration ratio is calculated as,

$$\text{Concentration ratio} = C/Cmax$$

The concentration rations were used to examine the mixing and distribution of pore water into the water column due to medusa pulsation.

The goal of this study is to study the fluid dynamics of medusa currents that for quantifying the distribution of pore water in the vertical water column for *Cassiopea* spp. Planar laser induced Fluorescence was performed to understand the bell kinematics and distribution of entrained pore water into water column. 2D particle image velocimetry was performed to study the hydrodynamic forces involved in the distribution. Both PLIF and PIV data were compared to examine the relative roles of advection and diffusion.

4.2 Material and Methods

4.2.1 *Cassiopea* spp. collection and handling

Cassiopea individuals of varying bell sizes were obtained from Carolina biological supply, NC, USA, during May 2016. Five individuals were used in this study with bell diameters ranging between 2 cm to 7 cm. The medusae were transported overnight and placed in a 20-gallon glass aquarium maintained at 20-24^{o}C with artificial salt water with salinity 1.024 g L^{-1}. The medusae were target fed live *Artemia* spp. nauplii for every two days. Metal halide lighting was used in the 20-gallon tank used for housing the medusa, and set to operate between 8-10 hours continuously on a daily basis. Submersible heaters were used to ensure the housing tank water was maintained at a temperature range of 20-24^{o}C. All experiments were conducted at room temperature during summer of 2016 (July and August).

4.2.2 Combined planar laser induced fluorescence (PLIF) and particle image velocimetry (PIV)

Planar Laser Induced Fluorescence (PLIF) technique was used to analyze the amount of pore water release due to *Cassiopea* pulsations. Experiment was performed in laboratory aquaria of 60.96 cm x 60.96 cm x 30.48 cm available in ATRC Laboratory 150. In aquarium tank, a special dyed sand bed was prepared with Rhodamine WT (Keystone Inc., IL, USA) of 21 cm x 21 cm x 1 cm height at the center of aquarium and undyed substrate bed of 2 cm above it, making substrate with total height of 3 cm. Water with salinity 1.025 g L^{-1} was used to fill the aquarium tank up to 22 cm above the substrate. 0.01 gm of Rhodamine dye (Keystone Inc., IL, USA) was added to make salt water in tank of known concentration of 2 x 10^{-4} g/L. A point source from ND:YAG double pulsed laser (New Wave Research, CA, USA) with wavelength 530 nm was converted to 2D planar sheet of thickness 5 - 6 mm using cylindrical lens (focal length = 20 mm) and was made to illuminate the flow field. Also a point source from a portable IR laser (2500mW) with wavelength 808 nm was converted to planar sheet of thickness 2-3 mm using cylindrical lens (focal length =10 mm) and was used to illuminate the flow field for PIV observation. The laser sheets were focused perpendicular to substrate along the diameter of medusa as shown in figure 1. High speed 1 mega-pixel CMOS camera (Phantom Miro LC110, Vision Research Inc., Wayne, NJ, USA) with 60 mm constant focal length lens (Nikon Micro Nikkor, Nikon Corporation, Tokyo, Japan) at frame rate of 32 Hz and full resolution of 1280 x 800 pixels was used to record the PIV observation. PLIF videos were recorded using sCMOS camera (LaVison GmbH, Gottingen, Germany) camera with full resolution of 2600 X 2200 pixels at a frame rate of 15 Hz. Double frame mode was used for recording PLIF images, with pulse separation time of 20 ms (time between two images in an image pair). An optical filter (550 nm long pass) was mounted on sCMOS camera lens to record the fluorescence intensity. Background video was recorded immediately after introducing the organism in the tank for each experimental run and dark images

were recorded with camera lens closed for PLIF calculations. Experimental setup is shown in Fig 18. Later 10 complete pulsing cycles of medusa were recorded after 10-minutes duration for each medusa with bell diameters 20- 60 mm.

All the recorded PLIF videos with 10 complete pulsing cycles were processed to get an averaged image at time point. These averaged PLIF images containing the intensity values were exported in ".png" format and further processed in MATLAB (The Mathworks, Inc., Natick, MA) program using formulation of Crimaldi, 2008. PIV videos were processed in the Davis 8.2 software (LaVision GmbH, Gottingen, Germany) to obtain the 2D velocity vector fields around individual with an interrogation window of 64 x 64 and 32 x 32 with 50% overlap and 2 passes each. Post-processing was performed by rejecting velocity vectors with peak ratio of less than 1.2 and interpolation was used to replace the empty vectors. These vector fields were averaged for 10 cycles and exported in .dat file format containing velocity information (horizontal velocity u and vertical velocity v) and momentum fluxes were calculated in MATLAB software (The Mathworks, Inc., Natick, MA). PLIF videos were also used to calculate the pulsing frequency of individual to relate the vertical forces F_y, velocity V, pulsing frequency f, and bell diameter d.

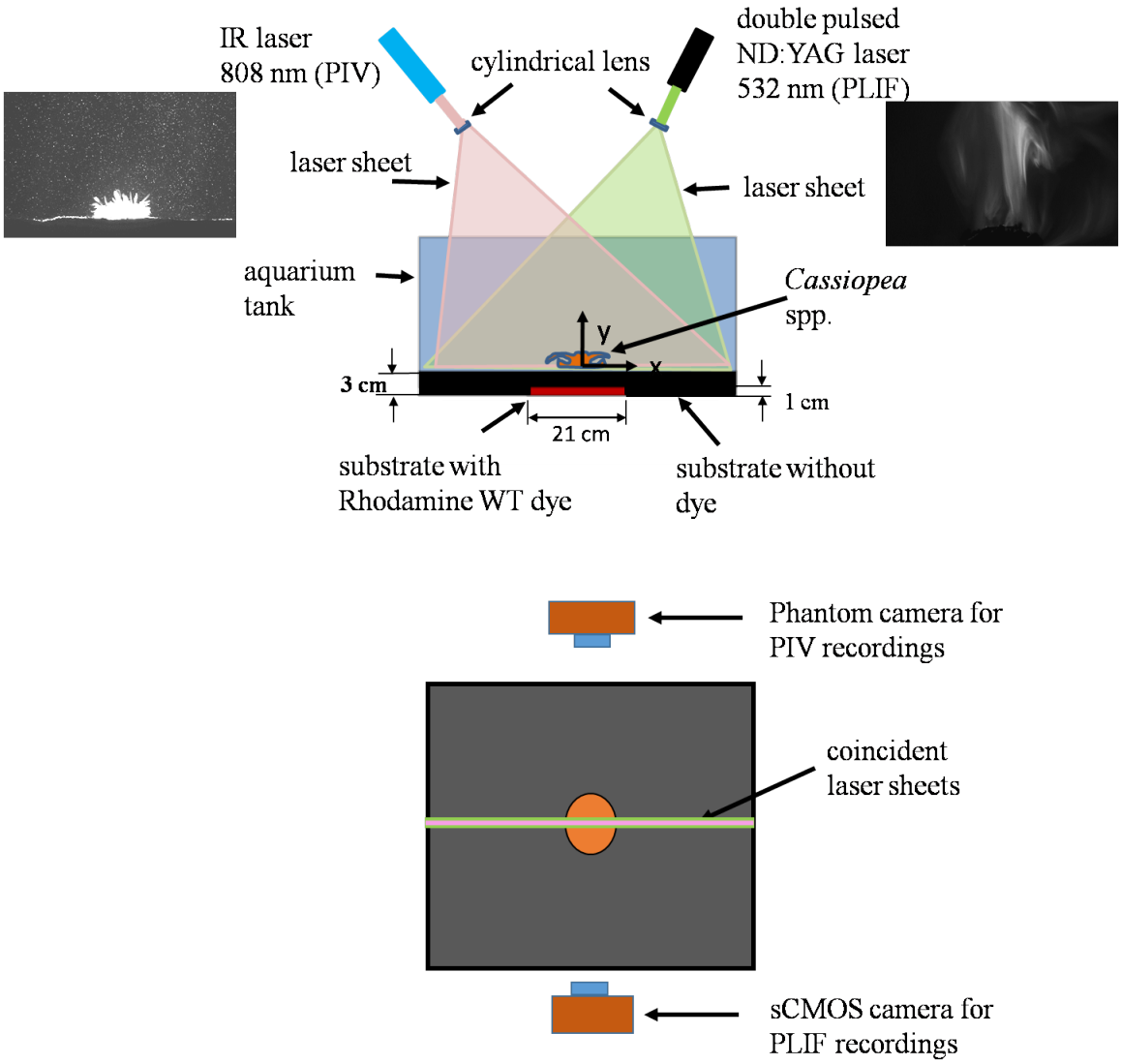

Figure 18. Experimental setup used for combined planar laser induced fluorescence (PLIF) and particle image velocimetry measurement. Top picture shows the front view and the bottom represent top view of the setup. Inserts: left hand side is a raw PIV image and right hand side is a raw PLIF image.

4.3 Results

4.3.1 Bell kinematics

Pulsing frequency of *Cassiopea* spp. were calculated from PLIF and PIV recordings for 10 pulsations. Pulsing frequency vs diameter was plotted as shown in Fig 19. Standard deviations of ± 0.02 Hz was noted for smaller medusa with bell diameter 2 cm. Medusa with near field data was having pulsing frequency of 0.9±0.01 Hz. The pulsing frequency decreased with increase in bell diameter.

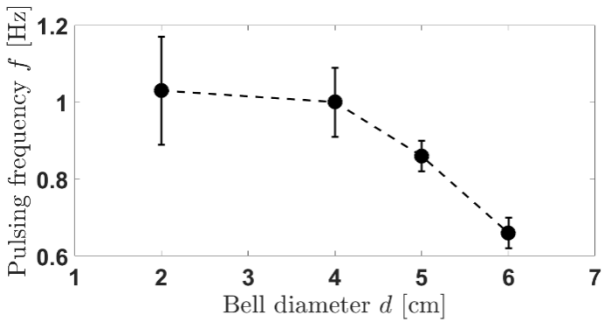

Figure 19. Pulsing frequency (f) vs bell diameter d with error bars. Medusa with 3 cm bell diameter was used for near field observation has pulsing frequency of 0.9 ± 0.01 Hz.

4.3.2 Phase-averaged flow characteristics

4.3.2.1 Concentration ratio

Far field PLIF videos were used to look into time averaged and time resolved characteristics. Averaged images of 10 complete pulsing cycles of each individual were processed to get the raw images as shown in Fig 20. These images were processed to obtain time averaged PLIF contour plot as shown in Fig 21. Color map shows the ratio of concentration available at corresponding pixel to maximum concentration entrained from substrate by the *Cassiopea* individual. Color bar shows value of 1 at the place of concentrated pore water. For medusa with bell diameters, the

C/C_{max} was found along the medusa current. Maximum concentration was found near the oral arms for the larger diameter medusa.

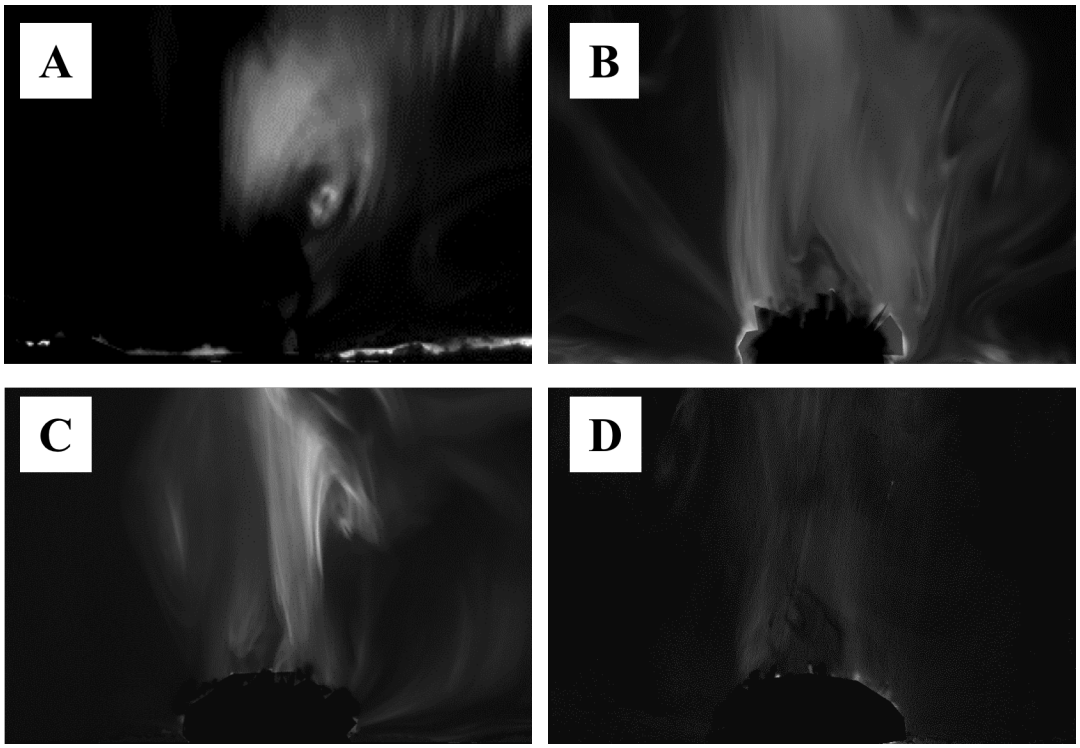

Figure 20. PLIF raw images following subtraction of background images for various bell diameters of d A) 2 cm B) 4 cm C) 5 cm and D) 6 cm.

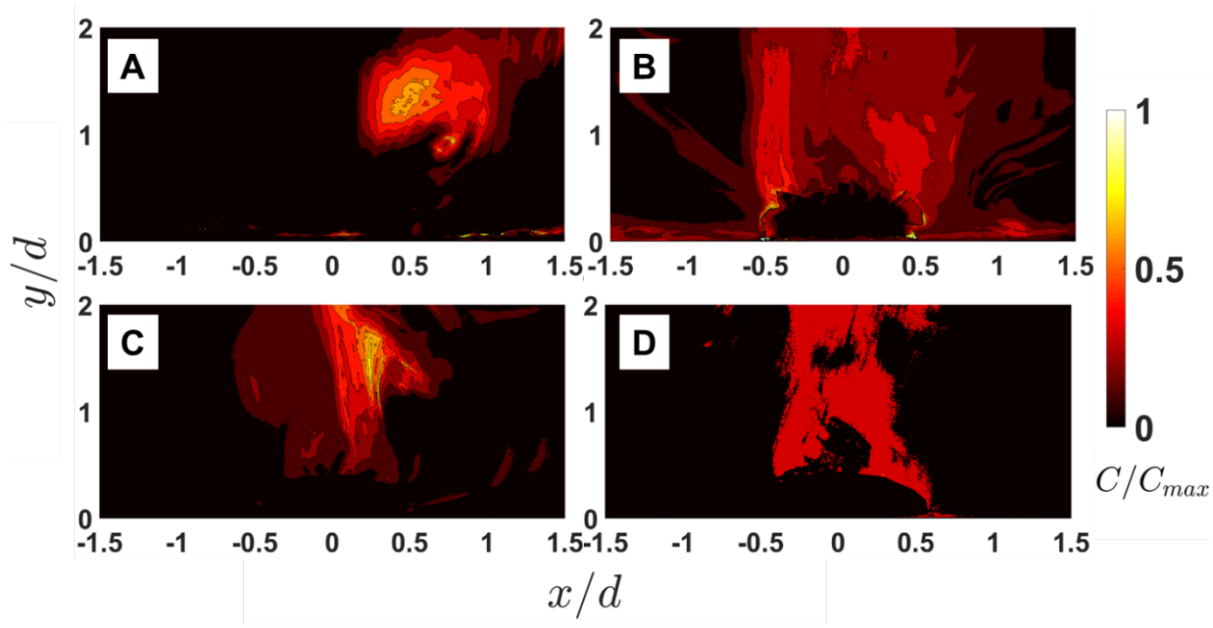

Figure 21. Processed background subtracted PLIF data with concentration ration, Concentration at each pixel divided by maximum concentration extracted by medusa (C/C_{max}), was plotted against non-dimensionalized x and y axis.

After obtaining these concentration contours, non-dimensioned concentration fluxes were measured for all medusae at y/d = 0.75 to 1.5 along -1.5 < x/d <1.5 as shown in Fig 22A. The extracted values from each diameter were plotted as shown in Fig 22B. These non-dimensioned fluxes were calculated at various vertical location of y/d = 0.75 to 1.5. The plot shows that for each individual, the value of non-dimensioned concentration flux increased from y/d = 0.75 to y/d =1.25 and later decreased at y/d = 1.5. While with increase in diameter, these values appear to change with pulsing frequency. For example, the pulsing frequency of 2 cm medusa was 1 Hz with highest standard deviation of d ± 0.2 Hz, so was the non-dimensioned concentration flux.

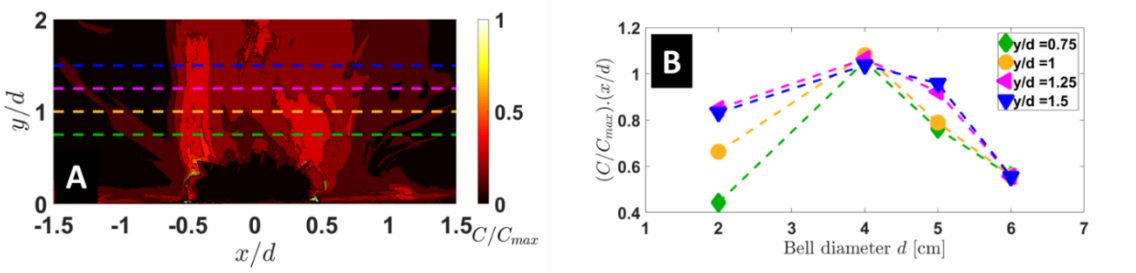

Figure 22.Concentration flux vs diameter. (A) Sample nondimensionalized concentration map showing the various locations of extraction of concentration fluxes calculated over -1.5 <x/d< 1.5. Each line with marker represent a y/d location. Diamond marker at y/d = 0.75, Circle marker at y/d =1, left triangle represent y/d = 1.25 and downward triangle represent y/d at 1.5.

4.3.2.2 Hydrodynamic force

Total force was measured at y/d = 0.75 to 1.5 in the MATLAB program to relate the pulsing frequency with hydrodynamic forces. The Fig 23 A shows the locations of force calculations i.e., at y/d =0.75 to 1.5. Fig 23B shows the calculated forces at given locations. For a 2 cm and 6 cm medusae, the total hydrodynamic force increased with increase in medusa current penetration. While for 4 cm and 5 cm medusae, the force increased till y/d = 1 and later decreased with increase in current penetration. The total measured force was due to the vertical force component obtained due to pulsing force.

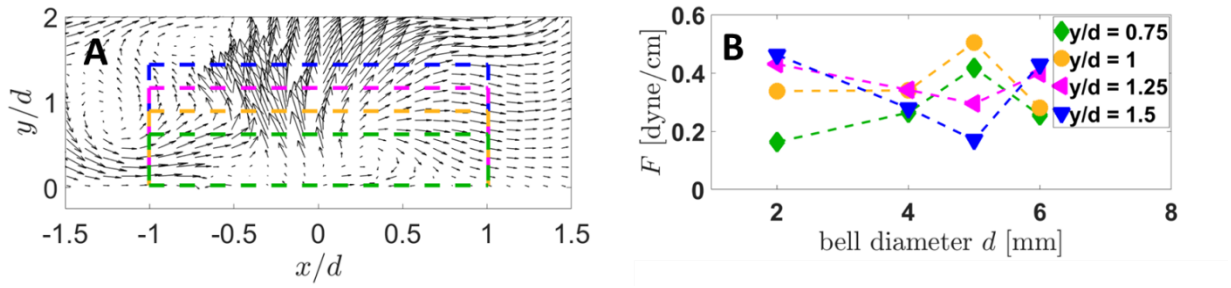

Figure 23. (A) Time averaged PIV vector field showing various y/d locations for a fixed x/d locations of + 1 d for a 4 cm medusa. (B) total hydrodynamic force measured at the given locations of y/d of 0.75 to 1.5. Standard deviation of ±0.03 to ±0.1 was obtained in hydrodynamic forces.

All the results showed the effect of pulsing force of each medusa in pore water exchange with vertical water column. In order to observe the changes in each cycle, time resolved analysis was made.

4.3.3 Time resolved Characteristics

4.3.3.1 Power stroke

PLIF plots were processed for near fields to look into the pore water entrainment. Pulsations of medusa, enhanced the dye release from the substrate near the bell tip and was pulled along its bell margin during the start of power stroke as shown in Fig. 24. As the power stroke progress from 0% PS to 33% PS, small vortex ring was formed as shown in Fig.24A. The vortex ring advances along the bell margin and increased in size at 66% PS as shown in Fig. 24C. At the end of power stroke a strong starting vortex was formed and was then pushed into vertical water column through oral arms as shown in Fig 24D. PLIF processed images are shown in Fig 25 from A-D at same percentage power strokes. Maximum concentration ratio was found along the vortex

structure. During the power stroke the previously formed vortex structure was pushed into the vertical water column and discretized into small flow structures as shown in Fig 25A-D.

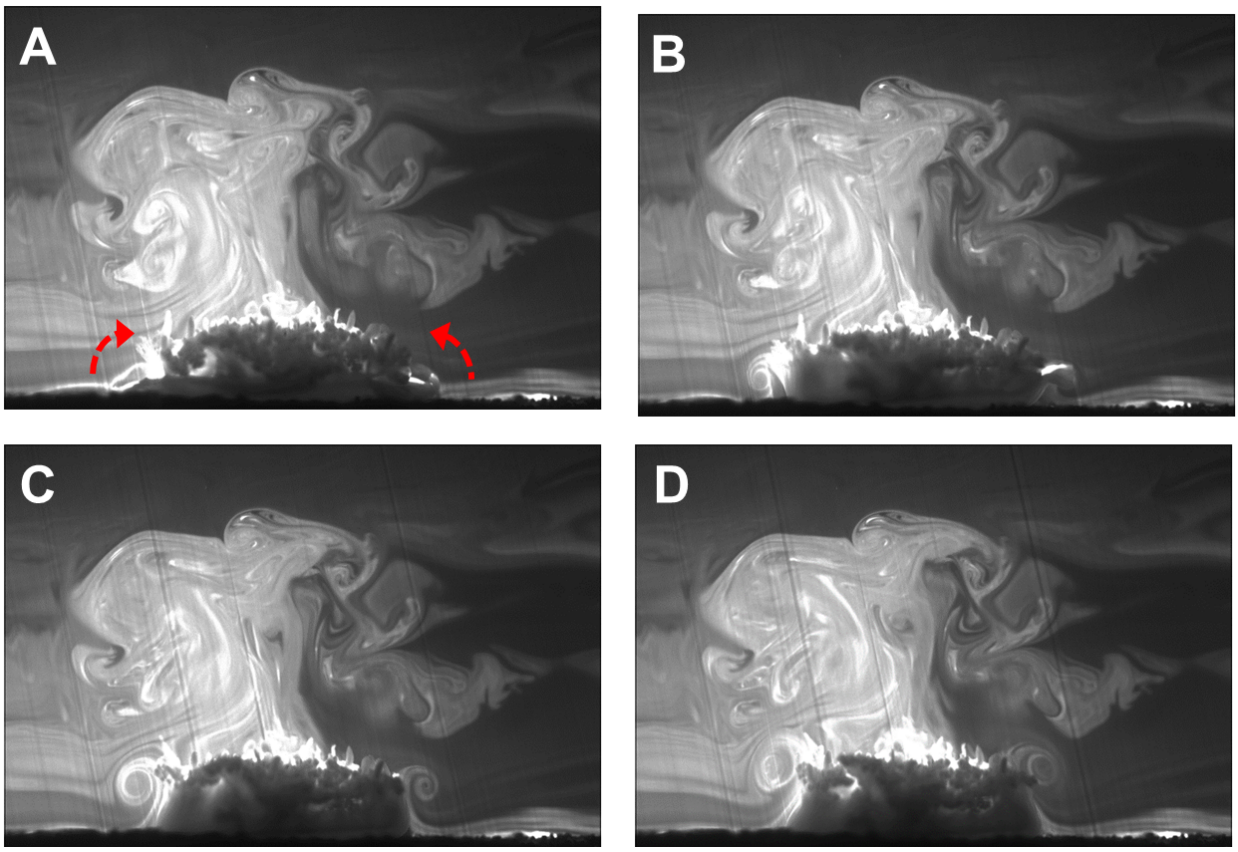

Figure 24. Near-field time-resolved PLIF raw data showing the 3 cm medusa power stroke. A) 0% PS B) 33% PS C) 66% PS D) 100% PS. Arrows in Fig A shows the motion of power stroke with time progress.

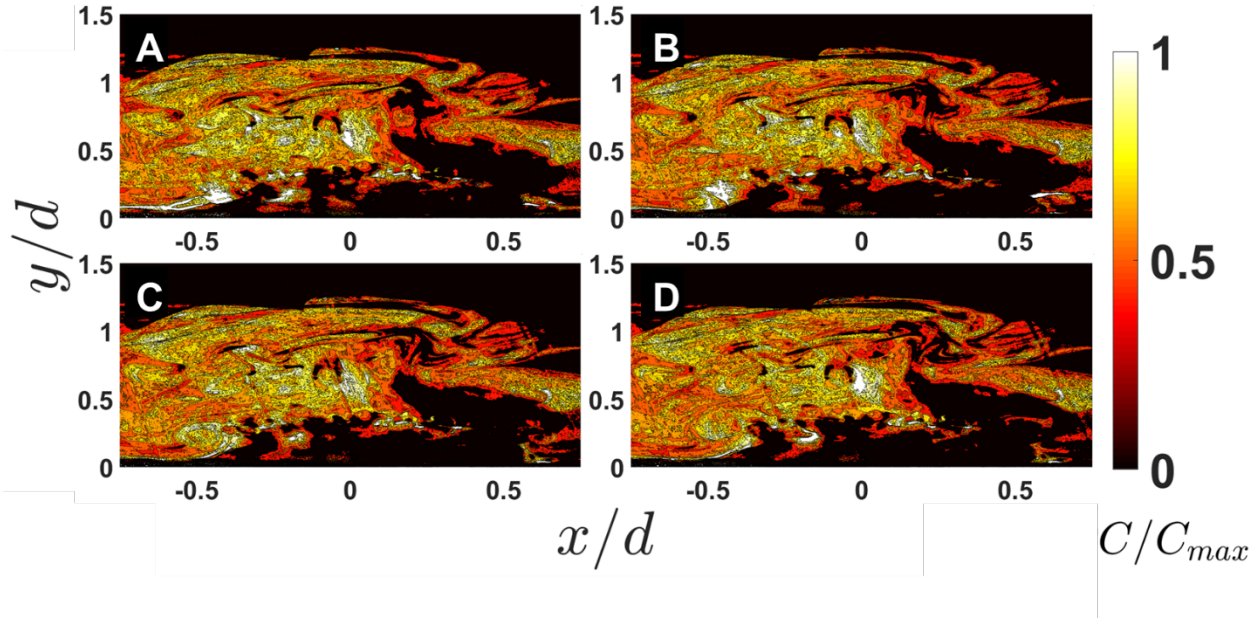

Figure 25. Near-field time-resolved PLIF concentration maps for 3 cm medusa at power stroke A)0% PS (B) 33% PS C)66% PS (D) 100% PS.

4.3.3.2 Recovery stroke

The vortex ring formed in the power stroke, advanced into the water column as the recovery stroke progressed from Fig 26 A – D. The dye entrained in this vortex ring was diffused and increased it length diameter as shown in Fig 26D. This increased vortex ring size indicate its spread due to the resistance offered to medusa current by the vertical water column. Processed PLIF images are shown in Fig 27 A-D for same percentage recovery stroke. The diffusion from vortex ring can been seen clearly through the PLIF processed images. For example, the value of concentration ratio was 1 in the vortex flow structure and it decreased to 0.8 as shown in Fig 27A-D.

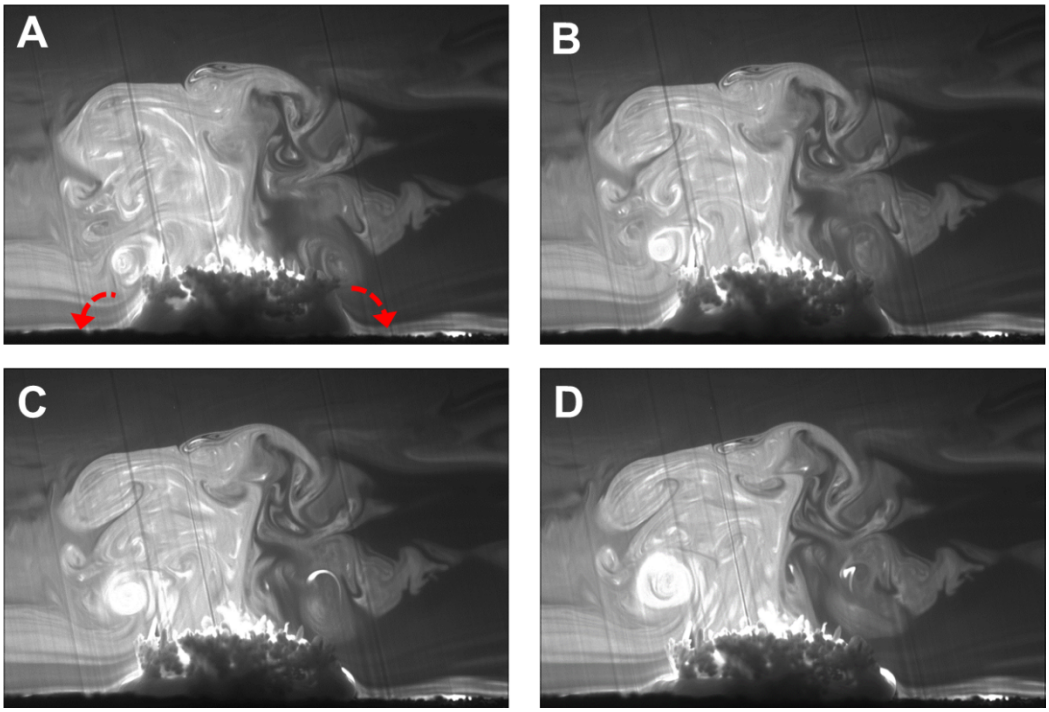

Figure 26. Near-field time-resolved PLIF images for 3 cm medusa during recovery stroke at (A) 0% PS (B) 33% RS (C) 66% RS (D) 100% RS. Arrows in the first image shows the direction of bell motion during the recovery stroke.

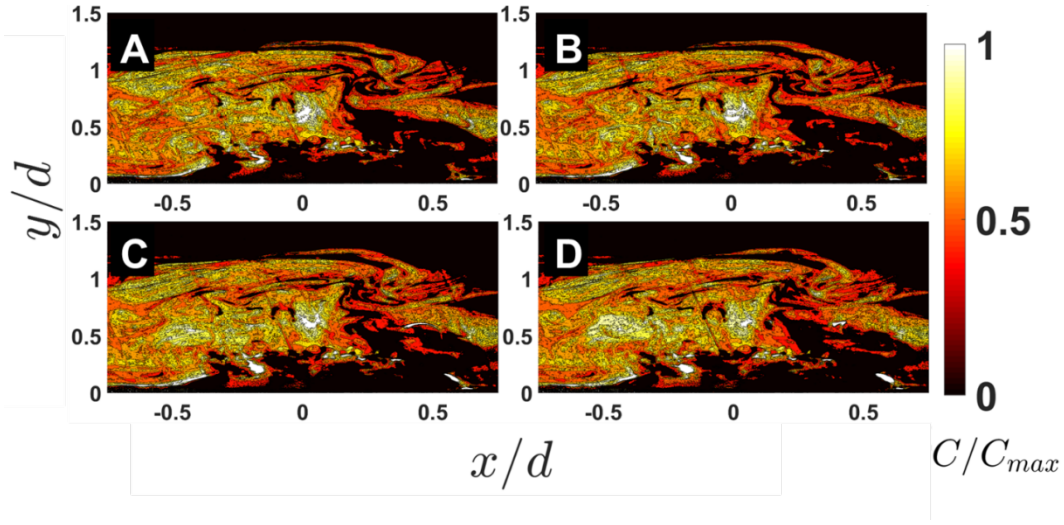

Figure 27. Near-field time-resolved PLIF concentration maps of 3 cm medusa during recovery stroke at A)0% B)33% C)66% D)100%.

4.3.3.3 Far-field 2D PIV

Time resolved far field PIV data was collected to observe the vorticity contours and also to extract the velocity profiles at desired locations. Fig 28 shows the time resolved PIV plots at various power stoke of 4 cm medusa. These plots shows the formation of vortex rings near the bell margin. As the power stroke starts as shown in Fig 28A, the fluid was pulled towards the bell margin from its surroundings including the pore water from substrate. As power stroke progress and reach 33%, the starting vortex was initiated as shown in Fig 28B. This starting vortex increased in strength and size at 66% as shown in Fig 28C. At the end of power stroke, this vortex was fully grown started to rise from the near substrate region as shown in Fig 28D. During the start of recovery stroke as shown in Fig 29 A, the vortex structure started to interact with the oral arms and start to lift into the medusa current. As recovery stroke reaches 33%, the stopping vortex was initiated due to the bell motion against the substrate as shown in Fig 29B. Recovery stroke at 66% was shown in Fig 29C and its stopping vortex decreased its strength and finally mixed with surrounding medium with no vortex ring presence as shown in Fig 29D.

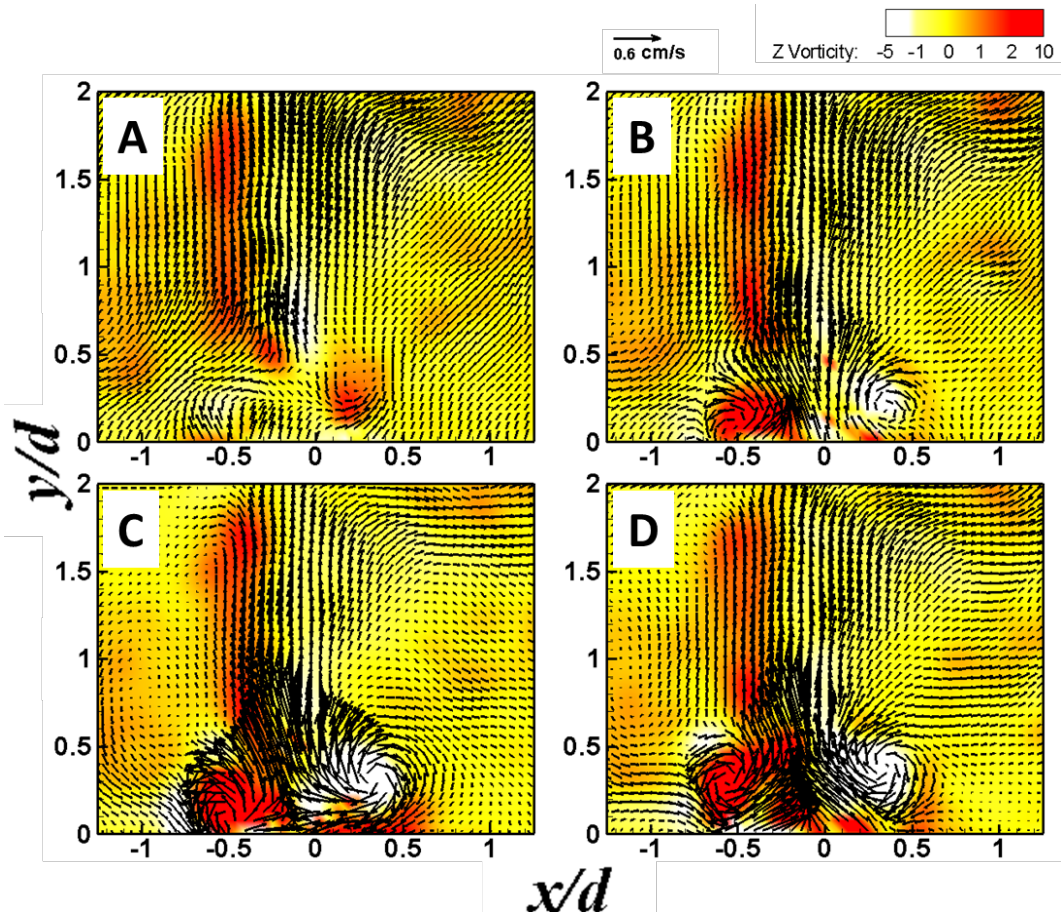

Figure 28. Power stroke time resolved PIV vorticity contours for 4 cm medusa at (A) 0% PS (B) 33% PS (C) 66% PS (D) 100% PS.

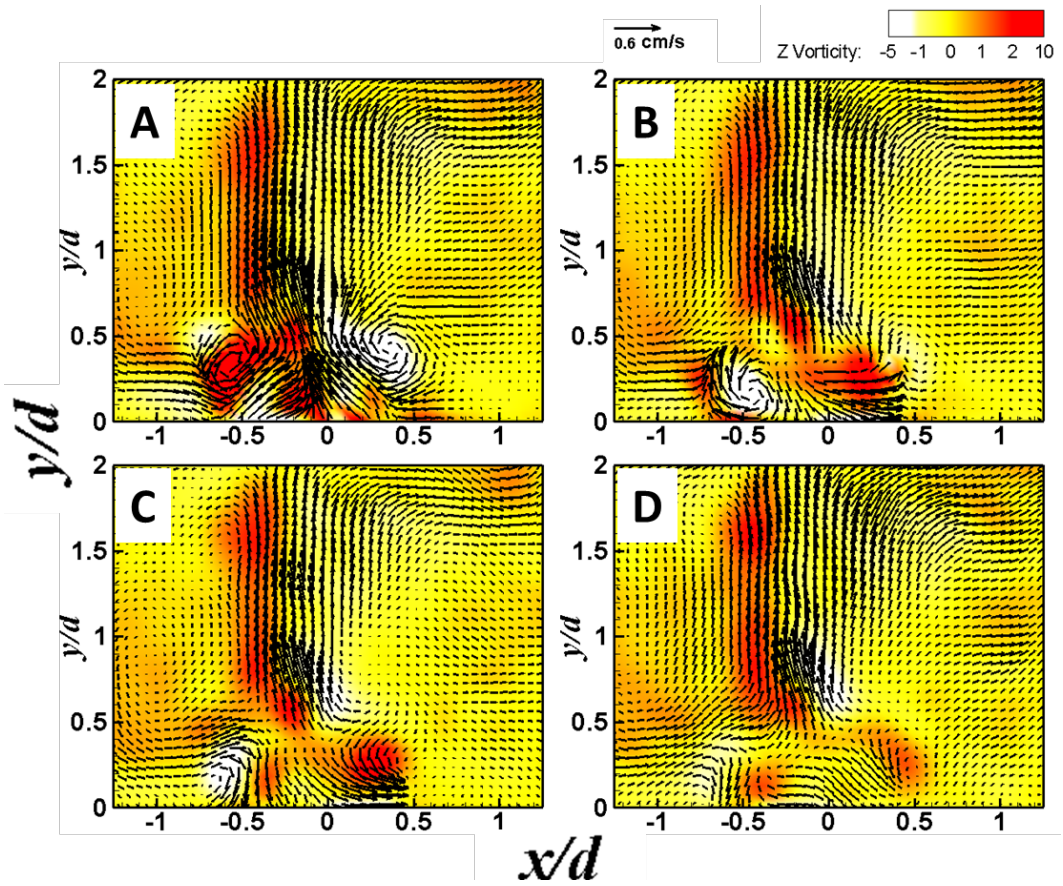

Figure 29. Time resolved PIV vorticity contours for 4 cm medusa recovery stroke at (A) 0% RS (B) 33% RS (C) 66% RS (D) 100% RS.

4.3.3.4 Far-field nondimensionalized concentration maps

For the same medusa of 4 cm, PLIF concentration contours were processed to look at the change in concentration ratio as the pulsation progress. Fig 30 shows the various concentration contours at 0%, 33%, 66% and 100% PS. Fig 31 shows the concentration contours for 0% , 33%,66%,100% RS. Concentrations values were extracted along various y/d locations to plot concentration profiles.

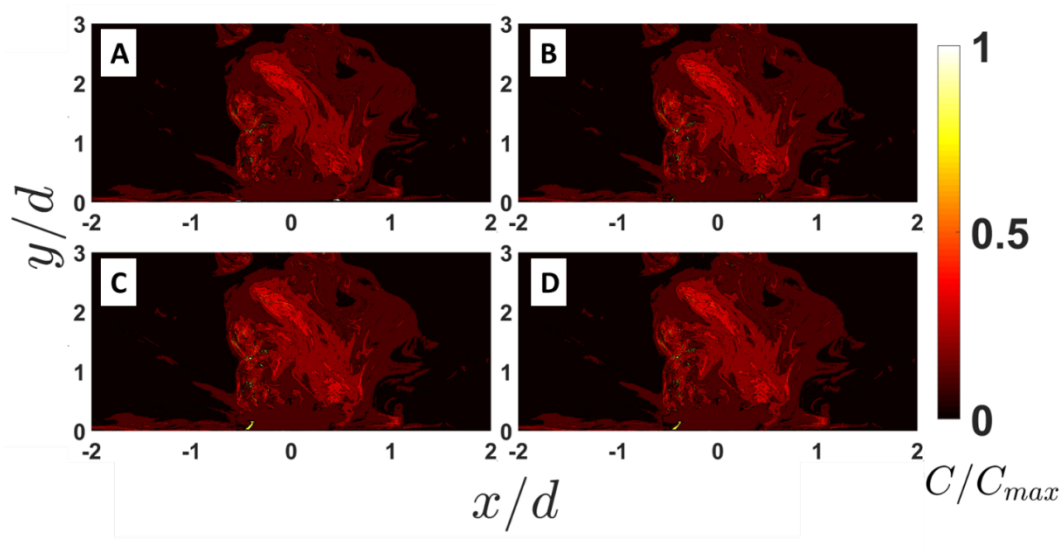

Figure 30. Far-field time-resolved nondimensionalised concentration maps for power stroke at A)0% PS B) 33% PS C)66% PS D)100% PS.

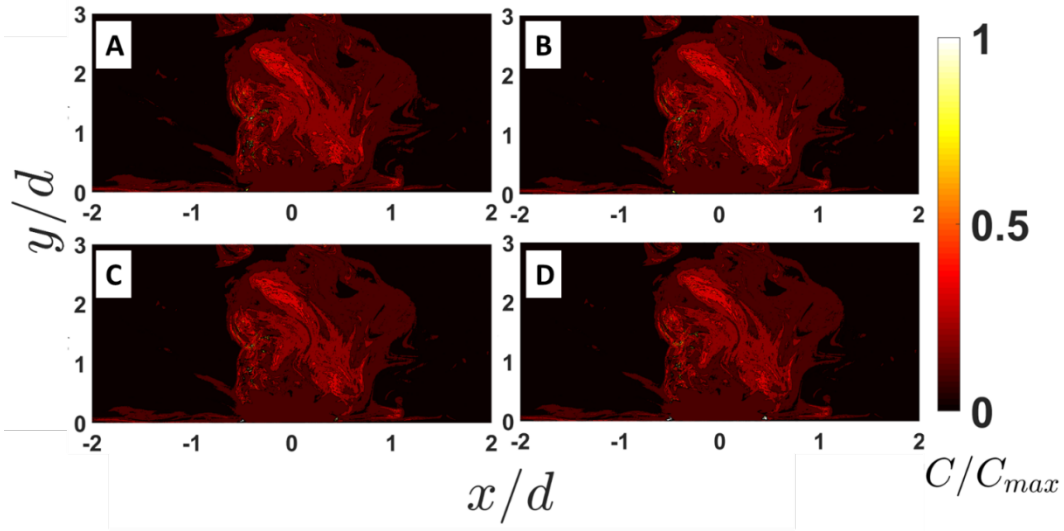

Figure 31. Far-field time-resolved nondimensionalised concentration maps for recovery stroke at A) 0% RS B) 33% RS C) 66% RS and D) 100% RS.

4.3.3.5 Far-field velocity profiles

From time resolved PIV plots, velocity vectors are extracted to look at the change in medusa current along the water column height and across the current. Also concentrations ratios along x/d -1.25 to 1.25 were extracted from far field PLIF plots of same medusa of 4 cm to plot concentration and velocity profiles as shown in Fig 32-33.

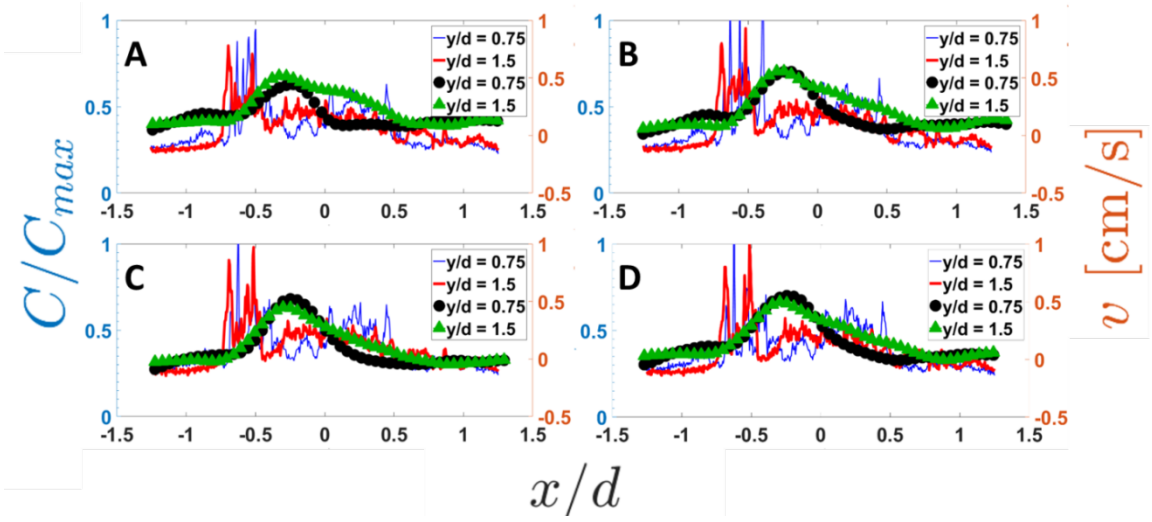

Figure 32. Concentration ratio profiles and velocity profiles during power stroke at A)0% PS B) 33% PS C)66% PS D)100% PS. Left axis represent concentration ratio, right y axis represent vertical velocity component v with x/d as x-axis. Thin (blue) and thick (red) lines (without markers) represent concentration ratio at y/d =0.75 and 1.5 respectively. Lines with circle and triangle markers represent vertical velocity at y/d = 0.75 and 1.5 respectively.

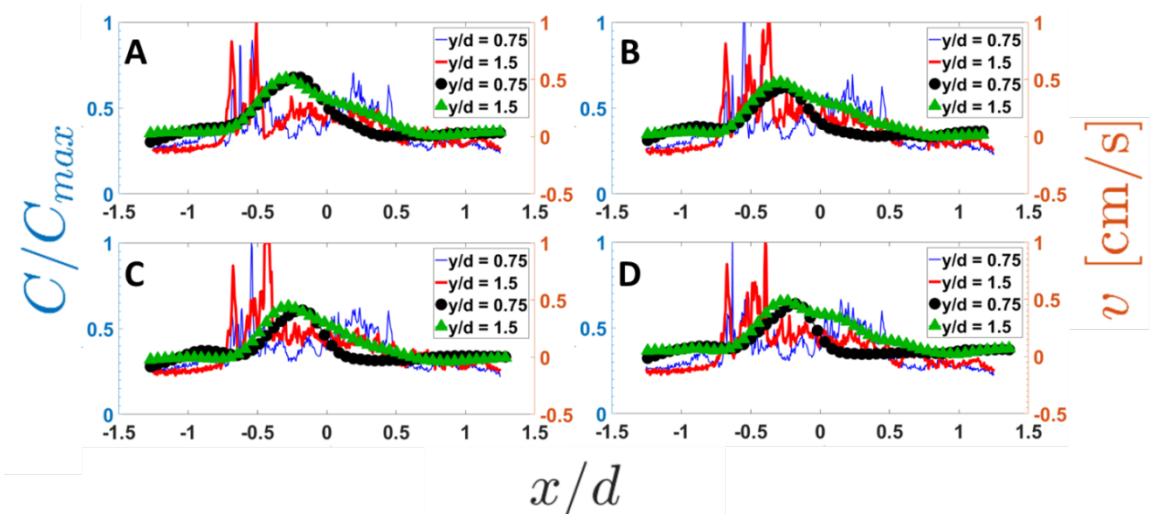

Figure 33. Concentration ratio profiles and velocity profiles during recovery stroke at A)0% RS B) 33% RS C)66% RS D)100% RS. Left axis represent concentration ratio, right y axis represent vertical velocity component v with x/d as x-axis. Thin (blue) and thick (red) lines (without markers) represent concentration ratio at y/d =0.75 and 1.5 respectively. Lines with circle and triangle markers represent vertical velocity at y/d = 0.75 and 1.5 respectively.

All the profiles appear to show a trend between the velocity and concentration. Vertical velocity increased as power stroke progress at y/d = 0.75 and later decreased in recovery stroke. The appearance of strong peaks in the concentration profiles were due to the present of flow structure with dye concentration. A similar trend of concentration was observed at 0.75 location. While the velocity at y/d = 1.5, remained with same peak value throughout the cycle and so was the concentration profile. This might happen due to the velocity that helps out in producing the force required to entrain the concentration.

4.3.3.6 Far-field time-resolved observations

Far field observation helps us to understand the advection of the vortex structures in the water column. As the power stroke progress in the far field observation, the vortex formed due to previous pulsation was pushed into water column and its spreading was observed as the medusa

current progress as shown in Fig. 34A-D. During recovery stroke, the vortex introduced into water column due to power stroke was pushed along the medusa current as shown from Fig 35A-D. The dye concentration in the vortex diffuses as time progress along the length of water column and diffueses.

When we observe three continous pulsing cycles as shown in Fig 36 advection of flow structures can be seen clearly. The flow structure namely vortex structure formed at power stroke passs through resistance network and convert to a flow struture. This flow structure was formed at the end of recovery stroke. This flow structure comes out oforal braches and enters the water along the medusa current. Fig 36A-C shows three continous 100% recovery strokes. The box with dashed lines (red box) shown in Fig 36 A show circumscribes the flow structure at the end of first recovery stroke. As the second cycle progress, new flow structure was formed as shown in thin box (yellow).During this cycle the previously formed flow structure named the one in dashed line box advected by small amount near 0.3d. As the pulsing cycle progress, the new flow structure was advected into the current circumcribed by thick box(cyan). During this cycle the, flow structure 1 was advected and diffused along the jet spreading. A similar pattern was seen in the medusa of 6cm diameter as shown in Fig 36 D-F. Conversion of large scale vortex into small scale flow structures was seen due to the shear resistance around the medusa current in the water column. So as the pulsation progress, the medusa adds the pore water entrained into water column during the recovery stroke. The resistance network of oral arms helps the vortex structure formed in power stroke to break into small flow structures by which the fluid is properly mixed with water column. Compared with smaller diameter the flow structure advection was more compared to smaller medusa and also the stretch of flow structure was more entailing the mixing nature of larger medusa to be high.

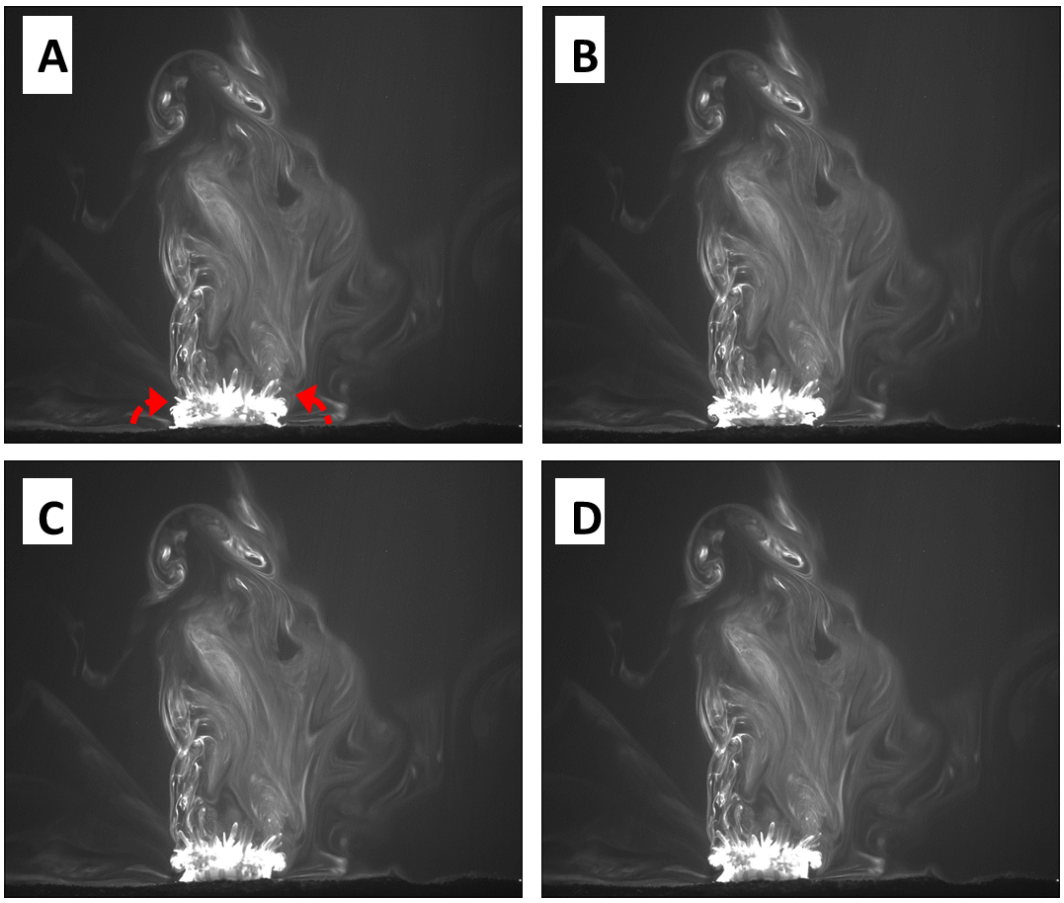

Figure 34. Far-field time-resolved PLIF data during power stroke of 4 cm medusa at A)0% PS B)33% PS C)66% PS D)100% PS to show the flow structure formation. Arrows indicate the direction stroke.

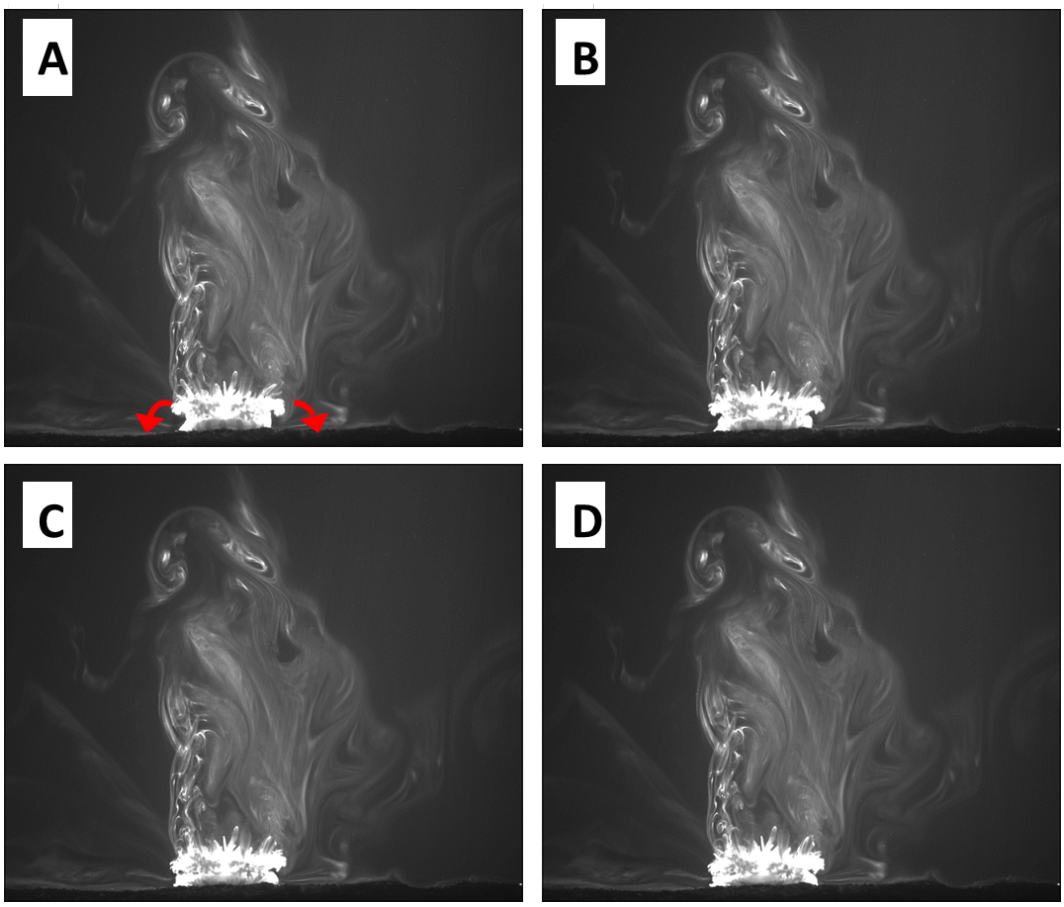

Figure 35. Time-resolved PLIF data during recovery stroke of 4 cm medusa at A)0% RS B)33% RS C)66% RS D)100% RS to show the flow structure formation. Arrows indicate the stroke direction.

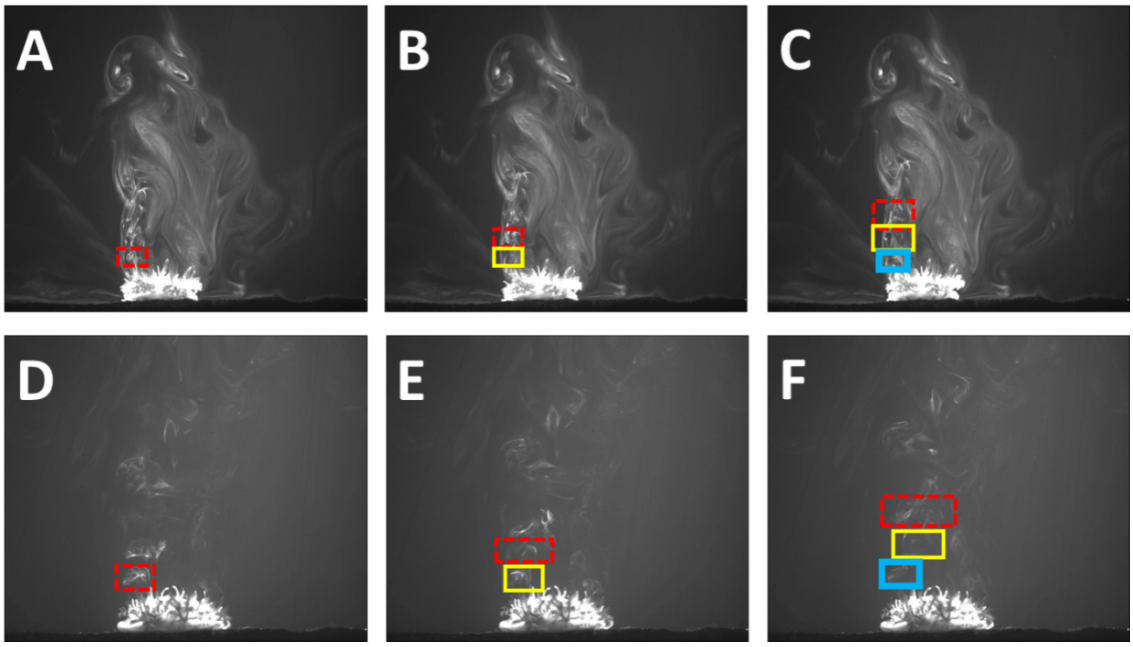

Figure 36. Far-field time-resolved PLIF unprocessed images showing flow structure advection at the end of recovery stroke. (100% recovery stroke) A) 4 cm medusa in cycle 1 B) 4 cm medusa in cycle 2 C) 4 cm medusa in cycle 3 D) 6 cm medusa in cycle 1 E)6 cm medusa in cycle 2 C) 6 cm medusa in cycle 3.

The pulsations of smaller and larger medusa showed displacement of flow structure by different length scales in the experiment. For smaller medusa, the flow structure formed at the end of power stroke was displaced by 0.5d when it reach 100% recovery stroke, it was displaced further by 0.3 d in the next pulsing cycle. While in the large medusa, the large medusa, the flow structure formed was displaced by 0.5 d in the first pulsing cycle and later by 0.2d. However, breaking of large flow structure into small flow structures (nearly circular) was observed. This formation was due to breakage of large vortex into small vortex by oral arm as shown in fig 37.

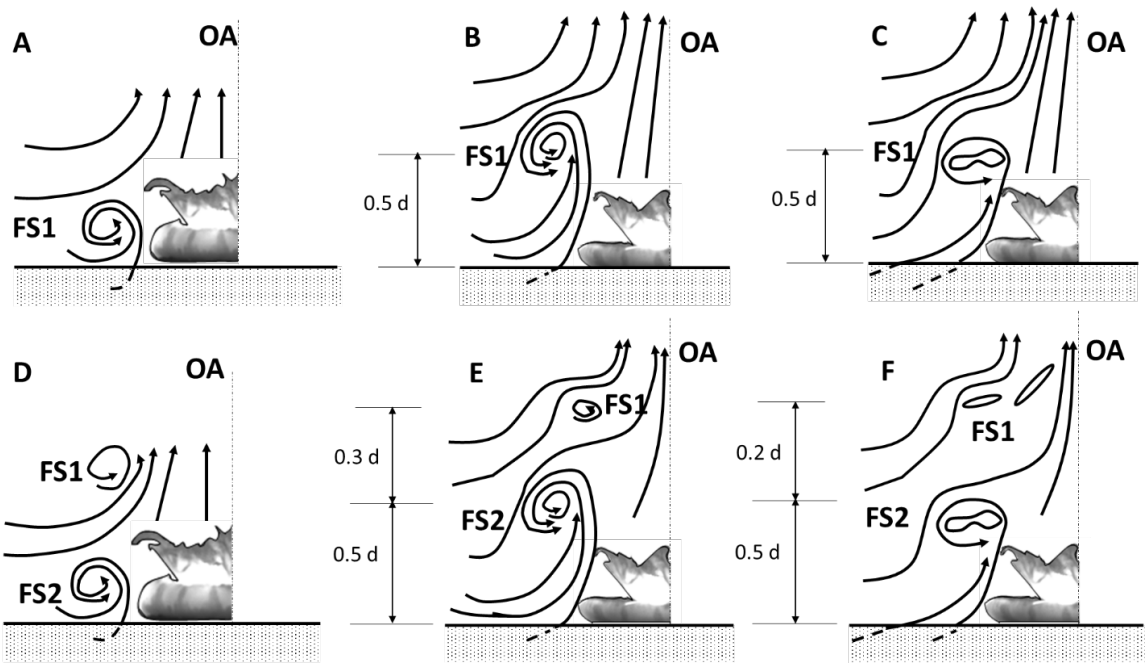

Figure 37. Pictorial representation of flow structures and their position at end of 100% power stroke and 100% recovery stroke in two continuous cycles for smaller medusa 4 cm and large medusa 6 cm bell diameters. (A) 100% PS cycle 1 for 4 cm medusa. (B) 100% RS for 4 cm medusa for cycle 1. C) 100% RS for 6 cm medusa for cycle 1 (D) 100% PS for 4 cm medusa cycle 2. (E) 100% recovery stroke for 4cm medusa cycle 2 (F) 100% recovery stroke for medusa cycle 2.

4.4 Discussion

Near field PLIF cycle raw images shows the entrainment of pore water from the substrate, its movement along the bell margin and finally into strong vortex structure near bell tip margin during the power stroke. This indicates that bell pulsations not only entrain the fluid along the substrate [33] but also from the substrate in the same flow structures. However, in far field PLIF images helps to understand the pore water mixing in the vertical water column. Large flow structure formed in the power stroke was pushed through the high resistance network of oral arms. Recovery stroke, which is longer than power stroke time period, helped the vortex structure to break into to smallest flow structure. Velocity profiles showed decrease in velocity peaks along the y/d indicating decrease in medusa current as the height of water column increase.

Concentration profiles and shear forces from currents showed direct relation with the velocity profiles. Thus when current penetrate into the water column, a strong shear force was found which decreased with water column height due to decrease in vertical velocity. Thus concentration available at given y/d depends on the medusa vertical velocity. This strong shear force produced through current can enhances the proper mixing and diffusion of pore water in local regions.

Pulsing frequency impacts the medusa current penetration. Current penetration increases with increasing pulsing frequency. Since time period is inversely proportional with frequency, power stroke frequency dominates recovery stroke frequency and greater pulsing force is induced on the flow structures. This increased force helps the increased jet penetration and also the mixing. However, pulsing frequency of an individual depends on the environmental conditions and its behavior.

In smaller medusa, due to the high pulsing frequency, the entrainment was more and the flow structures were repeatedly add to the water column. While the medusa with larger diameter, pulsate with lower frequency giving more time for recovery stroke and proper water mixing of flow structure. It is possible that each medusa can modulate their bell pulsation frequency based on their individual size (muscle mass) and generate mixing of nutrients in the water column. From an engineering perspective, studies on this organism could be useful for the design of unsteady suction pumps. Such pumps could be used for pisciculture (fish farming), where there is need of pore water containing minerals and nutrients extraction into water column. When *Cassiopea* grows in fish farms, they help by pumping the required nutrients but medusa even effect the growth of fishes by decreasing the food resources as medusa feed on shrimp [50], which is food for fishes. This alternative replacement of medusa with mechanical pump can help the fisheries.

PIV experiments on different medusa showed the effect of bell pulsations to be one diameter radially in all direction above the surface and so the present PLIF experiment has to be conducted with Rhodamine WT dye placed beneath substrate of more than 2 cm depth, with different depths of colored bed to understand the pulsation effect beneath the substrate to justify if the bell pulsation affect the pore water pumping just for 1 diameter or more.

4.5 Conclusions

Pulsations of *Cassiopea* medusae entrain the pore water from the bell-substrate interface in the form of vortex structure during power stroke and push it through the oral arms breaking it into small flow structures into the water column. PLIF investigations showed maximum concentration ratio was in the vortex structure. Flow structures were showed for a pulsing cycle in PLIF and PIV experiments. PLIF studies showed the smaller individuals pulsate frequently; add pore-water into the water column; and mix it properly. In contrast, the larger medusa pulsate less with large force and maintain proper pore-water mixing. Importance of oral arms was understood in breaking mixing of pore water into water column. Future investigations on the *Cassiopea* spp. were suggested to study the pulsing effect beneath the substrate.

CHAPTER V

SUMMARY

5.1 Study findings

Food is main source of energy. Organisms living in benthic layer use different techniques for prey capture as the surrounding medium as background velocities of 0-2 cm/s. Also there is increase in gelatinous biomass in the recent years and study on such biophysical interactions is required to understand the organism behavior. Experiments were performed to study the effect of background flows on the *Cassiopea* spp. and also to understand the pore water pumping in no background flow.

Bell kinematics showed decrease in pulsing frequency with increasing diameter. Qualitative flow visualizations helped to understand the formation of flow structures above the substrate. Investigations with addition of background flow showed formation of asymmetric vortices in smaller medusa and no starting vortex in the upstream of larger medusa. There was decrease in value of peak velocity vectors in flow structures with increase in medusa bell diameter and also with increase in the background flow. There was decrease in jet penetration due to decrease in vertical velocity which decreased with increase in bell diameter. The presence of oral arms make sure to break the vortex structure into small flow structures and also to provide more time scale for prey encapsulated vortex to stay long, thus increasing suspension feeding time scale.

Experiments with PLIF showed enhancement of pore water into vertical water column. The non-dimensional concentration flux for each individual showed an increase and decrease trend with increase in vertical column height. A similar pattern of increase and decrease in pulsing force was observed. Our experimental observations include the decrease in vertical velocity with increase in vertical height and also the concentration profiles appeared to follow the velocity profiles at each instant. The distance travelled by the flow structures during the pulsations were analyzed to understand the pore water mixing. The flow structure formed due to smaller medusa pulsation moved up to 0.5d in the first pulsation and travelled by 0.3d during the second pulsation in the form of small vortex structure. While the flow structure formed due to large diameter medusa pulsation was strong and travelled a distance of 0.5d during the first pulsation. The flow structure was later broken into small flow structures and travelled a distance of 0.2d approximately. This suggested that the larger medusae were capable of mixing the nutrients released from the pore spaces of the sand bed.

Finally, the smaller medusa pulsated more frequently and generated narrow jets above the oral arms under both conditions of with and without background flow conditions. This jet penetrated into the water column, generating larger shear in the background flow. In comparison, the large medusa pulsated less frequently, had lower wide peak velocity above the oral arms, providing less current penetration. Wider current ensures proper mixing of pore water into the vertical water column.

5.2 Limitations and challenges

In PLIF, the *Cassiopea* were tested on the same substrate made for the first experiment. So there is chance of scavenging the dye available by the first introduced organism. However, for this effect we have divided the concentration at each pixel with the maximum concentration available at that instant. Also, the PLIF experiments were previously conducted on steady state boundary

conditions while this is the first research with dynamic boundary conditions using the unsteady pulsing organism. We used image averaging for this unsteady pulsing effects. The present experiment was performed with a single set of experiments with increasing diameter. However more experiments are required to make proper conclusions and to provide statistics of such pore water mixing. PLIF and PIV in chapter four were performed at offset of 5 min due to lack of resources. However, the simultaneous, PLIF and PIV will quantify, the results more accurately.

5.3 Recommendations for future studies

The limited number of *Cassiopea* individuals used in this study did not allow for statistical analysis. Future studies should include a larger variation in bell diameters than reported in this thesis, including multiple individuals per bell diameter group. Finally, *Cassiopea* live in fairly dense aggregations. PIV and PLIF measurements developed in this study can be used to study pore water pumping in groups and the possibility of synergistic interactions in pulsation patterns between neighboring medusae.

REFERENCES

[1] https://en.wikipedia.org/wiki/Aquatic_predation.

[2] Bartleson,R.D.,"*Interactions of seagrass beds and the water column: effects of bed size and hydrodynamics",Univ. of Maryland, 2004.*

[3] Riisgård, H.U., and Larsen,P.S., "Particle capture mechanisms in suspension-feeding invertebrates," *Marine Ecology Progress Series,* vol. 418, pp. 255-293, 2010.

[4] Monismith,S.G. and Koscf,J.R. " A study of model bivalve siphonal currents," *Limnology and oceanography,* vol. 35, pp. 680-696, 1990.

[5] O'Riordan, C.A., Monismith,S.G., and Koseff,J.R. , "The effect of bivalve excurrent jet dynamics on mass transfer in a benthic boundary layer," *limnology and oceanography,* vol. 40, pp. 330-344, 1995.

[6] Riisgård, H.U.; Thomassen, S.; Jakobsen, H.; Weeks, J. M.; Larsen, P.S., "Suspension-feeding in marine sponges halichondria-panicea and haliclona-urceolus-effects of temperature on filtration rate and energy- cost of pumping," *Marine Ecology Progress series,* vol. 96, pp. 177-188, 1993.

[7] Vogel, S., "Current-induced flow through the sponge,Halichondria," *The Biological Bulletin,* vol. 147, pp. 443-456, 1974.

[8] Hunter, T., "Suspension Feeding in Oscillating Flow: The Effect of Colony Morphology and Flow Regime on Plankton Capture by the Hydroid Obelia iongissima," vol. 176, pp. 41-49, 1989.

[9] Ferner, M.C., and Gaylord, B., "Flexibility foils filter function: structural limitations on suspension feeding," *The Journal of Experimental Biology,* vol. 211, pp. 3563-3572, 2008.

[10] Shenker, J.M., "Carbon content of the neritic scyphomedusa Chrysaora fuscescens," vol. 7, no. 2, pp. 169-173, 1985.

[11] Brodeur, R.D., Mills, C.E., Overland, J.E., Walters, G.E., and Schumacher, J.D., "Evidence for a substantial increase in gelatinous zooplankton," *Fisheries Oceanography,* vol. 8, no. 4, pp.

296-306, 1999.

[12] Purcell, J.E. and Sturdevant, M.V., "Prey selection and dietary overlap among zooplanktivorous jellyfish and juvenile fishes in Prince William Sound, Alaska," *Marine Ecology Progress Series,* vol. 210, pp. 67-83, 2001.

[13] Templeman, M.A. and Kingsford, M.J., "Trace element accumulation in *Cassiopea* sp. (Scyphozoa) from urban marine environments in Australia.," *Marine Environmental Research,* vol. 69, pp. 63-72, 2010.

[14] Al-Rousan, S., Rasheed, M., and Badran, M., "Nutrient diffusive fluxes from sediments in the northern Gulf of Aqaba, Red Sea," *Scientia Marina,* vol. 68, no. 4, pp. 483-490, 2004.

[15] Porter, J., Kosmynin, V., Patterson, K., Porter, K., Jaap, W.C., Wheaton, J., Hackett,K., Lybolt,M., Tsokos, C., Yanev, G., Marcinek, D., Dotten,J., Eaken,D., Patterson,M., Meier, O., Brill, M., and Dustan, P., "Detection of Coral Reef Change by the Florida Keys Coral Reef Monitoring Project, The Everglades, Florida Bay, and Coral Reefs of the Florida Keys, 2002.

[16] LaBarbera, M., "Feeding currentsand Particle Capture mechanisms in suspension feeding animals",*American Zoologist,* Vol. 24, pp. 71-84, 1984.

[17] Reiswig, H.M., "Partcile feeding in natural populations of three marine demosponges," *Biol. Bull.,* vol. 141, pp. 568-591, 1971.

[18] Reiswig, H.M., "The aquiferous systems of three marine demospongiae," *J. Morphol,* vol. 145, pp. 493-502, 1975.

[19] Riisga˚rd, H.U., and Larsen,P.S., "Minireview: Ciliary filter feeding and bio-fluid mechanics-present understanding and unsolved problems," *Limnol. Oceanogr.,* vol. 46, no. 4, pp. 882-891, 2001.

[20] Larsen,P.S., and Riisgåd, H.U., "The sponge pump," *Journal of Theoretical Biology,* vol. 168, no. 1, pp. 53-63, 1994.

[21] Reece, J.B., urry, L.A., Cain, M.L., Wasserman, S.A., Minorsky, P.V. and Jackson, R.B., An Introduction to Invertebtrates, Pearson Education, Inc. , 2011.

[22] Winter, J.E., "A review on the knowledge od suspension feeding in Lamellibranchiate bivalves,with special reference to artficial aquaculture systems," *Aquaculture,* vol. 13, pp. 1-33, 1978.

[23] Drinnan, R.E., "An apparatus for recording the water pumping behaviour of Lamellibranchs," *Netherlands J of sea research,* vol. 2, no. 2, pp. 223-232, 1964.

[24] Niggl, W., and Wild,C., "Spatial distribution of the upside-down jellyfish *Cassiopea* sp. within fringing coral reef environments of the Northern Red Sea: implications for its life cycle," vol. 64, pp. 281-287, 2010.

[25] Arai, M., "Pelagic coelenterates and eutrophication: a review," vol. 451, pp. 69-87, 2001.

[26] Brusca, R.C., and Brusca, G.J., "Invertebrates," vol. 23, no. 4, pp. 974-976, 2003.

[27] Arai, M., A Functional Biology of Scyphozoa, London: Chapman & Hall, 1997.

[28] Jantzen, C., Wild, C., Rasheed, M., El-Zibdah, M., and Richter, C., "Enhanced pore-water nutrient fluxes by the upside-down jellyfish *Cassiopea* sp. in a Red Sea coral reef," *Marine Ecology Progress Series,* vol. 411, pp. 117-125, 2010.

[29] Todda, B., Thornhillb, D.J., and Fittb, W.K., "Patterns of inorganic phosphate uptake in *Cassiopea* xamachana: A bioindicator species," vol. 52, pp. 515-521, 2006.

[30] Fitt, W.K. and Costley, K., "The role of temperature in survival of the polyp stage of the tropical rhizostome jellyfish *Cassiopea* xamachana," vol. 222, p. 1998, 1998.

[31] Hofmann, D.K., Neumann, R. and Henne,K., "Strobilation, budding and initiation of scyphistoma morphogenesis in the rhizostome *Cassiopea* andromeda (Cnidaria: Scyphozoa)," vol. 47, pp. 161-176, 1978.

[32] http://thescyphozoan.ucmerced.edu/Biol/Ecol/LifeHistory/ScyphozoaLH.html.

[33] Santhanakrishnan, A., Dollinger, M., Hamlet, C.L., Colin, S.P. and Miller, L.A.,"Flow structure and transport characteristics of feeding and exchange currents," *The Journal of Experimental Biology,* vol. 215, pp. 2369-2381, 2012.

[34] Hamlet, C., Santhanakrishnan, A., Miller, L.A., "A numerical study of the effects of bell pulsation dynamics and oral arms on the exchange currents generated by the upside-down jellyfish *Cassiopea* xamachana," *Journal of Experimental Biology,* vol. 214, pp. 1911-1921, 2011.

[35] Hamlet, C.L. and Miller, L.A., "Feeding currents of the upside down jellyfish in the presence of background flow.," *Bull Math Biol,* vol. 74, pp. 2547-2569, 2012.

[36] Huettel, M., Ziebis, W., and Forster, S., "Flow-induced uptake of particulate matter in permeable sediments," *Limnol. Oceanogr.,* vol. 41, no. 2, pp. 309-322, 1996.

[37] Parr,A.D., Richardson, C., Lane, D.D., and Baughman,D., "Pore Water Uptake by Agricultural Runoff," *Journal of Environmental Engineering,* vol. 113, no. 1, pp. 49-63, 1987.

[38] Precht, E., and Huettel, M., "Advective pore-water exchange driven by surface gravity waves and its ecological," *Limnol. Oceanogr,* vol. 48, no. 4, pp. 1674-1684, 2003

[39] Philp, J.L., Jaffrin, Y.M., and Ding, L., "Hemolysis During Membrane Plasma Separation With Pulsed Flow Filtration Enhancement," *J Biomech Eng 116(4), 514-520 (Nov 01, 1994) ,* vol. 116, no. 4, pp. 514-520 , 1994.

[40] Maze, B., Tafreshi, H.V., Wang, Q., and Pourdeyhimi, B., "A simulation of unsteady-state filtration via nanofiber media at reduced operating pressures," *Journal of Aerosol Science,* vol. 38, no. 5, pp. 550-571, 2007

[41] Shimeta, J., and Jumars, P.A.," Physical mechanisms and rates of particle capture by suspension feeders," *Oceanogr. Mar . Biol . Annu . Rev .,* vol. 29, pp. 191-257, 1991.

[42] Welsh, D.T., Dunn, R.J.K., and Meziane,T., "Oxygen and nutrient dynamics of the upside down jellyfish (*Cassiopea* sp.) and its influence on benthic nutrient exchanges and primary production," *Hydrobiologia,* vol. 635, pp. 351-362, 2009.

[43] Fleck, J. and Fitt, W.K., "Degrading mangrove leaves of rhizophora mangle Linne provide a natural cue for settlement and metamorphosis of the upside down jelly fish *Cassiopea* xamachana bigelow," *The Journal of Experimental Marine Biology and Ecology,* vol. 234, pp. 83-94, 1999

[44] Vogel, S. and LaBarbera, M., "Simple Flow Tanks for Research and Teaching," *BioScience.,* vol. 28, pp. 638-643, 1978.

[45] Hedrick, T.L., " Software techniques for two and three dimensional kinematic measurements of biological and biometrric systems," *Bioinspir. Biomim,* vol. 3, 2008.

[46] Gordon, M. and Soria, J.P., "PIV measurements of a zero-net-mass-flux jet in cross flow," *Experiments in Fluids ,* vol. 33, pp. 863-872., 2002.

[47] McFadden, C.S., "Colony fission increases particle capture rates of a soft coral: Advantages of being a small colony," vol. 103, no. 1-3, pp. 1-20, 1986.

[48] Jsrgensen, C.B., "Fluid mechanical aspects of suspension feeding," vol. 11, pp. 89-103, 1983.

[49] Crimaldi, J.P., " Planar Laser INduced Fluorescence in aqueous flows. -," *Exp Fluids,* vol. 44, pp. 851-863., 2008 .

[50] Purcell, J.E. and Arai, M.N.,"Interactions of pelagic cnidarians and ctenophores with fish :a review", vol 451, pp.27-44, 2001.

GLOSSARY

Substrate

Surface on which living organisms dwell is called substrate. Depending on size of particulates, there are different types of substrates which include Mud (diameter <1 mm), Sand (diameter 1-2 mm), Granule (diameter 2-4mm), Pebble (diameter 32-64mm), Cobble (diameter 64-256 mm) and Boulder (diameter >256mm).

Benthic layer, Benthos and Benthic zone

Layer of water just above the substrate in water body is called benthic layer. The living organisms in the benthic layer are called Benthos. Benthos include both plants (flora) and animals (fauna). Ecological region containing substrate, benthic layer and benthos is called Benthic zone.

Bell diameter

Diameter of *Cassiopea* sp. bell at its relaxed position is called bell diameter (d).

Power stroke [PS]

Power stroke of the *Cassiopea* sp. is defined as the movement of bell from relaxed position to center of medusa. During power stroke the flow around the medusa is pulled towards the bell with initiation of vortex that is moving into the bell and flow is entrained into the subumbrellar region by pushing the bell against the substrate

Recovery stroke [RS]

Recover stroke of *Cassiopea* sp. is defined as the movement of bell from center of medusa axis against the substrate. During this stroke the flow entrained from power stroke is pushed through the oral arms and expelled through the bell with formation of stopping vortex which is moving outwards from bell.

Pulsation

Combination of power stroke, recovery stroke and pause between them is called a pulsation or a cycle. The vortex structure formed during the power stroke entrains the prey particles. Thus during a pulsation water (containing prey) around the medusa is pulled towards the bell margin and pushed through oral arms for prey capture by oral arms as a current.

Pulsing frequency

Pulsing frequency is defined as number of pulsations per unit time. Pulsing frequency varies with each individual bell diameter and surrounding conditions. The pulsing frequency increased during the feeding process and also when chemical conditions of water changed.

APPENDIX A

Matlab code for PLIF processing

Followig function was defined to obtain the concentration at each pixel
Using Crimaldi, 2008.

```
function imageproc (startimage,endimage)

%This function processes images taken by the sCMOS camera which is a 16 bit camera. The function does processing defined by John Crimaldi where a background image is taken, a dark image is taken, and a set number of useful images is also taken. The algorithm subtracts out the background image (back)on a pixel to pixel basis and then divides by the background-dark (back-dark) images which gives the level of background concentration in the flume. This normalization is then multiplied by the mean of the background concentration [mean(back-dark)] to give pixel intensities over the entire imaging area. The output is then saved as a 16-bit image with values between 0 and 4095. All non integer values calculated are truncated while saving to unsigned 16 bit integer values. Input start image is image number to begin processing and end image is last image to process Output name is input image name with a preceding "n"


global im nim back dark a b

for i=1

   h=[0];
   head=int2str(h(i));            %Input image sequence numbers to loop

%--------------set constants-------------------------------------------------------
if h(i)<10
   header=['B0',head];
else
   header=['B',head];                    %Header image file name
end
```

```
rowsave=800;                              %Number of rows to save in processed output image
locr='cd C:\Users\manikantam\Desktop\test';                  %Location of raw images
locp='cd C:\Users\manikantam\Desktop\test';     %Location to save processed images
pedestal=40;                        %Pixel pedestal to add to images to prevent <0 values
%-------------------------------------------------------------------------------
%input background and dark images
eval(locr);                       %Changes directory to raw image location
back=imread('back','png');
%imshow(back);
dark=imread('dark','png');
back=double(back);
dark=double(dark);

%input images
k=0;
for i=1 %%give numbers based on the image you want to process
  eval(locr);                     %Changes directory to raw image location
  k=k+1;
  frame(k)=i;
if i<10
    imagenum=[header,'00',int2str(i)];
elseif i<100
    imagenum=[header,'0',int2str(i)];
else
    imagenum=[header,'',int2str(i)];
end
  im = imread(imagenum,'png');

  proc=['Processing image ',imagenum];
  disp(proc)

%Create images of non-processed data
colormap(hot)
clim=[0 500];
figure(1)
imagesc(im(:),clim);
%imshow(im);%Display Raw Image
im =double(im);
k=1:rowsave;
imagesc(im(k,:),clim)

%Calculate Processed Image data

mb=mean(mean(back(k,:)-dark(k,:)));
nim =mb*(im(k,:)-back(k,:))./(back(k,:)-dark(k,:))+pedestal;


%Limit pixel size to 12-bit, 0 to 4095
[a,b]=find(nim>4095);
c=size(a);
for d=1:c
```

```
  nim(a(d),b(d))=4095;
end
nim(1:2,:)=0;                %Rows 1 and 2 seem to have bad data so set to zero

%Plot Processed Images
figure(3)
colormap(hot)
nim=uint8(nim);
colorbar();
caxis([0 ;0.0025]);
imagesc(nim(1:rowsave,:),clim)
name=['f',imagenum,'.png'];
eval(locp)                %Changes directory to where processed images should be saved
imwrite(nim(1:rowsave,1:988),name,'compression','none')     %Save processed images as uint8
pause(0.1)

end
end
```

Step -2

Dividing the concentration at each pixel by maximum concentration entrained by *Cassiopea* during experimental run. Maximum value is obtained using maxin variable from each image

```
clear all
for i=1

   h=[0];
   head=int2str(h(i));          %Input image sequence numbers to loop

%--------------set constants-------------------------------------------------------
if h(i)<10
   header=['fB0',head];
else
   header=['fB',head];                  %Header image file name
end
                            %Number of rows to save in processed output image
locr='cd C:\Users\manikantam\Desktop\test';                  %Location of raw images
locp='cd C:\Users\manikantam\Desktop\test';     %Location to save processed images

k=0;
for i=1 %%change based on image to be processed
  eval(locr);                  %Changes directory to raw image location
  k=k+1;
  frame(k)=i;
  if i<10
    imagenum=[header,'00',int2str(i)];
  elseif i<100
    imagenum=[header,'0',int2str(i)];
  else
    imagenum=[header,'',int2str(i)];
```

```
   end
   a = imread(imagenum,'png');
a =double(a);

maxin(i) = max(a(:)); %%maximum intensity in the experimental run
finalimage = a /(0.9*255)%(maxin(i)));%255);%
final =finalimage;
j=1;
maaa=max(a(:))

check(i) = mean(final(:));

for p=1:1:988; %%change
   mfx(:,[j])=final(:,[p]) ;   %%concentration matrix for variable x-axis position
   j=j+1;
 end
ncols=988; %%change based on the number of pixels available in image
nrows=800;  %%change on the number of pixels available in image in row
for r = 1:nrows
   for c = 1:ncols

      if mfx(r,c) <= 0.3 %% for removing the intensity effects of medusa
         mfx(r,c) =0.0;

      end
      if mfx(r,c)>= 1 %% cannot exceed 1, as we divide with maximum concentration entrained
         mfx(r,c)=1;
      end
   end

end


 d=40 %% bell diameter in mm (need our input)
 x=-(83.91/d):(193.76/d)/(988-1):(109.85/d);  %% x-axis scale distribution (can change based on
input)
 y =(158-158/800)/d:-(158/800)/d:0;   %% Y axis scale distribution (can be changed based on
input)
mfx2=mfx

%% Display output and saving

figure(1)
hold on
contourf(x,y,mfx2);
colormap(hot);
set(gca,'fontsize',18,'fontweight','bold');
axis([-2  2 0 3]);
h=colorbar();
str3='$$ C/C_{max}$$';
title(h,str3,'interpreter','latex','fontsize',42,'fontweight','bold')
```

```
 locate = get(h,'title');
  pos = get(locate,'position'); %it gives a position of 0.0500 2.900 1.0001
pos(1,2) = pos(1,2)-80;
pos(1,1)   =    pos(1,1)+50
set(locate,'pos',pos);


caxis([0 ;1]);
str1='$$x/d$$';
str2='$$y/d$$';
xlabel(str1,'interpreter','latex','fontsize',42,'fontweight','bold')
ylabel(str2,'interpreter','latex','fontsize',42,'fontweight','bold')
set(gca, 'FontSize', 42);
box on
%pause();
 filename = sprintf('test_image_%d.png', i); %% saving image
  saveas(gcf, filename, 'png');


end
```

VITA

MANIKANTAM GOUD GADDAM

Candidate for the Degree of

Master of Science

Thesis: CURRENTS GENERATED BY UPSIDE-DOWN JELLYFISH: IMPLICATIONS FOR SUSPENSION FEEDING AND PORE WATER PUMPING

Major Field: Mechanical and Aerospace Engineering

Biographical:

Education:

Completed the requirements for the Master of Science in Mechanical and Aerospace Engineering at Oklahoma State University, Stillwater, Oklahoma in December, 2016.

Completed the requirements for the Bachelor of Engineering in Mechanical Engineering at Osmania University, Hyderabad, India in 2014.

Professional Memberships: Member of American Physical Society